Master's thesis
Master's Programme in Materials Research

# Wireless ultrasonic system for pipeline defect localization

Peetu Ihalainen

December 18, 2024

Supervisor(s): Professor Ari Salmi

Examiner(s): Professor Ari Salmi
Professor Edward Hæggström

University of Helsinki
Faculty of Science

P. O. Box 64 (Gustaf Hällströmin katu 2)
00014 University of Helsinki

HELSINGIN YLIOPISTO — HELSINGFORS UNIVERSITET — UNIVERSITY OF HELSINKI

| Tiedekunta — Fakultet — Faculty | Koulutusohjelma — Utbildningsprogram — Degree programme |
|---|---|
| Faculty of Science | Master's Programme in Materials Research |

Tekijä — Författare — Author

Peetu Ihalainen

Työn nimi — Arbetets titel — Title

Wireless ultrasonic system for pipeline defect localization

| Työn laji — Arbetets art — Level | Aika — Datum — Month and year | Sivumäärä — Sidantal — Number of pages |
|---|---|---|
| Master's thesis | December 18, 2024 | 48 |

Tiivistelmä — Referat — Abstract

In English:

In this thesis, I developed a measurement system that consists of wireless devices. The system measures defects on pipe structures by utilizing guided waves that propagate in the pipe. Each wireless device is capable of both exciting and recording signals and relaying the information about the propagating waves to a server.

I will explain in this thesis a high level description of the system as well as a simple use case where the system was successfully used to localize defect in a pipe.

The system was evaluated by installing 5 of the developed devices on a stainless steel pipe with a diameter of 154 mm and wall thickness of 2 mm. The pipe was intentionally defected to various degrees by grinding during the measurement. Between the individual grindings, the devices were used to transmit and record guided waves that were propagating in the pipe between each of the units.

The recorded signals were compared against simulated results obtained by fast algorithm developed for this system. The simulations yielded a domain which displayed the most probable location for the damage with each of the damage levels.

It was possible to localize the damage with the proposed design and algorithm in this case. By combining the devices and the fast algorithm the system could be used to continuously and in real time localize damage in a pipeline.

Suomeksi:

Tässä maisterintutkielmassa kehitin mittausjärjestelmän, joka koostuu langattomista laitteista. Järjestelmä mittaa putkessa ilmenevää vahinkoa. Sen toiminta perustuu putkessa kulkeviin ohjattuihin aaltoihin. Jokainen langaton laite pystyy sekä lähettämään, että vastaanottamaan ohjattuja aaltoja ja välittämään ne palvelimelle.

Tämä työ sisältää laitteiston toiminnan kuvauksen, kuvauksen esimerkkikäyttökohteesta, josta laitteilla kerättiin tuloksia, sekä näiden tulosten avulla esitetyn vahingon paikallistamisen.

Laitteiston toimintaa kokeiltiin asentamalla viisi yksikköä kiinni teräsputkeen, jonka läpimitta oli 154 mm ja seinämän paksuus 2 mm. Putkeen tuotettiin hiomalla vahinko, jonka syvyyttä kasvatettiin mittauksen aikana. Kunkin hionnan jälkeen laitteet mittasivat putkessa kulkevat ohjatut aallot kunkin yksikön välillä.

Putkesta mitattuja signaaleja verrattiin tietokoneella simuloituihin mahdollisiin vahingon sijainteihin. Simuloinnit tuottivat kartan, joka osoitti mahdollisen vahingon sijainnin putkessa kullakin vahingonasteella.

Vahingon paikallistaminen oli mahdollista käyttäen kehittämääni järjestelmää. Yhdistämällä laitteet ja kehittämäni nopea algortimi voisivat mahdollistaa reaaliaikaisen ja jatkuvan vahingon paikallistamisen putkissa.

Avainsanat — Nyckelord — Keywords

Non-destructive evaluation, ultrasound, guided waves

Säilytyspaikka — Förvaringsställe — Where deposited

Muita tietoja — Övriga uppgifter — Additional information

# Contents

# 1. Introduction

This work describes a fast deployable and low-cost network of wireless devices that monitors the quality and integrity of a pipeline by transmitting and recording guided waves propagating in the pipe wall. The location of the inconsistencies is determined by the time-of-flight (TOF) differences of the waves propagating from the transmitter to the receiver. This method is known in the literature as through transmission or pitch-catch method.

Usually, both in the literature and in the industrial applications, the integrity evaluation of the structures is done by equipment that is both expensive and usually not very easily portable. In this work, I will present a method for carrying out continuous and affordable wireless method to monitor structure integrity over time. The idea is to have a low-cost battery-powered device that can be attached to the pipeline permanently and wirelessly measure the pipe with any measurement interval ranging from minutes to months. The affordability of a single unit means that a higher spatial resolution can be achieved on even large scale objects as the sensors can be placed with a smaller spacing on the pipe, and on arbitrary angles, while keeping the total price low.

The main focus in this thesis is on the system design, especially the electronics, and localization algorithm.

The developed system was tested by placing 5 of the designed devices on a steel pipe to monitor the integrity of the pipe. First, a baseline measurement was carried out on the unaltered pipe. The pipe was intentionally damaged by grinding different levels of defects into it. A simple algorithm was programmed for the localization. When the algorithm was used with the data collected from the system, relatively good localization was achieved, depending on the damage severity.

Single unit was priced at 30 euros. The design work took place in years 2021 to 2022, which was a very turbulent period in the semiconductor market. This caused high variations in both the price and the availability of the integrated circuits that were used in the prototyping and final proposed design of the devices. The devices were given the nickname Relatively Affordable Ultrasonic Sensor (RAUS), and the units will be referred to by this name throughout this thesis.

The programming in this project consisted of C programming on the small wireless devices and Python programming to create the server and data handling environment. Finally, Matlab R2020b was used for data analysis.

## Defect localization in the literature

The oldest method for systematic pipe line integrity testing over long distances is the use of "pigs". Pigs were originally just simple rag packs that were launched in the pipe line to clear it from any residues that had accumulated in the inner walls. Pig blocks the flow inside the pipe and the pressure behind it grows larger and pushes it forward to the region with lower pressure. Some sources claim that pigs got their name from the acronym "pipe inspection gauge", others claim that the name comes from the squealing the device makes while it is travelling through the pipeline [1]. Since they were originally put to large scale use in the 1940's, they have been developed from just blocks of cloth that cleared the pipe line from fouling into sophisticated pipe monitoring devices with a variety of sensors. A modern pig is displayed in figure 1.1. The methods used to monitor the pipeline integrity by the modern pigs are camera

**Figure 1.1:** Modern pig in a cut-away pipe section, Creative commons

based, magnetism based or ultrasound based. Gas lines are a big market for such devices due to monitoring needs over hundreds of kilometers of pipe. In such case a probe that travels inside the pipeline provides a very accurate way to localize structural weaknesses, these include dents, pipe diameter changes etc[2]. One of such modern pig is proposed by Sampath *et al*[3]. Pipe line inspection by data collection with pigs is the most widely used method in the industry and there is a variety of companies providing pigging services.

One major drawback when using pigs is that they usually require a constant diameter pipeline and the device must be inserted inside the line. This is not always possible in the industrial environment, or even if it would be possible the insertion could require down-time of the pipeline in question. In such cases, integrity evaluation from outside of the pipeline is required. This thesis explores the current external evaluation methods and provides a method to investigate the pipeline integrity with the proposed design.

A lot of research has been published in the field of external pipeline defect and fouling localization. This is due to the fact that pipes are used in the industry to various extent to transport fluids in an effective manner from one location to an other. Pipelines carry many liquids and gasses that are essential for modern everyday life e.g. water, natural gas and refrigerating coolants. These systems can run for distances up to hundreds of kilometers and may be damaged from an external source, intentionally or accidentally, or from internal stress, for example over-pressure or fatigue [4]. Material integrity testing can prevent leaks or localize them in case the pipe is already leaking but the pipeline is long or buried underground and visual inspection is not possible [5].

The most common and industrially accepted method for external pipeline integrity evaluation in modern times is using a ring of transducers that is placed around the pipe.[6] The rings are made of some tens of discrete transducer elements. Channels are transmitting and receiving ballistic and some low order helical guided wave modes as they travel on the pipe. Any change in the pipe integrity or loading, caused by e.g. fouling inside the pipe or crack in the pipe wall, will cause the signal to propagate differently when compared to a pipe section in good condition. The method can be used to probe the pipe section between the transmitter and the receiver. An example set-up displaying this method can be seen in figure 1.2 by Lais *et al.* [7].

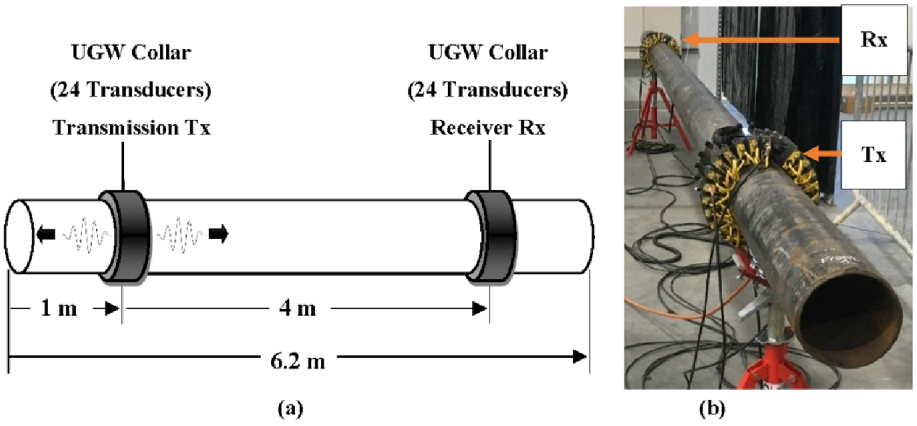


**Figure 1.2:** An example set-up of transducer ring on a pipeline[7]

The ring transducer probing has become very popular in the industry because of

the high signal to noise ratio they can achieve even in noisy environments. The major drawbacks is the time consuming installation of the rings, which must be repeated every time a new section of the pipeline is to be evaluated. Also the usage of a large amount of expensive piezo electric transducers, with necessary amplifier electronics, drive the price of the system high.

Another example of a modern ultrasound based defect localization is presented in the work by Raisutis *et al.*[8]. In their publication they were able to determine the fouling location in a steel pipe by scanning along the pipe surface and inspecting the dispersion curves of the arriving waves. They were able to show in frequency domain how the defect affects the dispersion curve. Here, instead of having multiple physical transducer they were using a single transducer to probe from multiple locations. This method can be less expensive as there is not a need for many transducers, but the measurement time will be longer. Users of such methods must also be careful that they have a precise control over the location of the probe and that the do sample from enough locations. If the spatial coverage is not sufficient, the wave number resolution in the two-dimensional Fourier transformation will be poor which results in a poor localization in return.

There are also alternatives to guided waves, one example is displayed in the publication by Zafiri *et al.*[9]. They propose a design which is an extremely low-power device which monitors the coating thickness on the pipe wall through accurate capacitance measurements. They claim that reduction in the coating thickness causes corrosion to damage the pipe, however, this sort of device can only monitor the pipe in narrow space, very locally.

The design proposed in this thesis displays a device capable of measuring in between the probes to cover bigger spatial visibility with lower amount of sensors. The proposed design evaluates the pipe that is between the sensors on any helical path, so with enough precision it can evaluate any point between two ultrasonic sensor units. The price of a single unit is designed to be low enough that one can place them permanently on the pipeline for continuous monitoring.

In the work by Santos *et al.* [10] a method for combined eddy current-ultrasonic non-destructive localization on hot piping was presented. They were able to localize defects in pipe structures at temperatures of 200 deg C using the ultrasonic system and up to 300 deg C using the eddy current method. These sort of temperatures are really meaningful in the industry and it would be interesting to see what kind of changes it would take to make the device presented in this thesis to work in elevated temperatures. Objects with even higher temperatures must be probed in non-contacting manner. An example use case for combined EMAT-laser ultrasound evaluation method is presented in the thesis by Rohani [11]. High temperatures are however outside of the scope of

this thesis and the work focuses on pipes at room temperature.

# 2. Theory

This theory section contains a short description of the guided waves found in the literature as well as their use in the defect and damage localization in metal structures. Also, the interaction of the structural defects on the guided wave propagation is explored.

## 2.1 Guided waves

Guided waves are mechanical waves that can exist in confined structures i.e. in any structure that is not infinite bulk. Guided waves occur when the mechanical properties of the material change at a boundary. For example, when a longitudinal wave hits a boundary with differing acoustic impedances.[12] Guided waves can be used to non-destructively evaluate (NDE) e.g. pipes filled with water,[13], pipes filled with gas, [14], or solid structures that consist of more than one material e.g. inserts,[15], or layered composite materials, [16]. Interest in using guided waves is due to their low attenuation compared to longitudinal and shear waves. This property is acquired by utilizing the object to be inspected as a wave-guide. For relatively thin structures the most widely used guided waves are Lamb waves.

### 2.1.1 Lamb waves

The theory behind the Lamb waves were initially published by Horace Lamb in 1917. Lamb waves propagate in thin structures. Lamb waves are a special case of Rayleigh waves, which are waves that propagate along one side of a solid structure. Lamb waves occur when the thickness of the structure is thin enough for the reflected wave from the bottom of the structure to be observable on the top layer. The Lamb waves can

be presented in an isotropic media with the following equations[17]:

$$\frac{\tan(dq)}{\tan(dp)} = -\frac{(k^2-q^2)^2}{4k^2qp}, \text{ for anti-symmetric modes}$$

$$\frac{\tan(dq)}{\tan(dp)} = -\frac{4k^2qp}{(k^2-q^2)^2}, \text{ for symmetric modes} \tag{2.1}$$

$$q^2 = \frac{\omega^2}{c_s^2} - k^2, \qquad p^2 = \frac{\omega^2}{c_l^2} - k$$

Isotropic means that the media is mechanically homogeneous in all spatial directions, and is used as an ideal case approximation for metals. Here $d$, $\omega, c_l, c_s$, are the plate thickness, angular velocity and longitudinal and shear sonic speeds of the material, respectively. $k$ is the wave number, defined as the ratio between the angular frequency and the phase velocity of the wave. These equations describe the fundamental dispersive nature of the Lamb waves; The speed of the wave is always dependent on its frequency.

## 2.2 Trigonometry in pipes

Because pipes are in essence plates whose longitudinal sides are connected, Lamb waves can be used to probe pipes, and the theory of plate waves can be applied to pipe structures. One can also visualize a pipe as a plate structure whose axial boundaries are connected, by adding virtual domains on top and bottom of the domain that represent the actual pipe dimensions, as illustrated in figure 2.1. The zeroth order helical path, or the ballistic path, is the path along which the wave travels the shortest distance between the transmitter and the receiver. The higher order helical paths travel around the pipe multiple times before reaching the receiver. These higher order modes are given the order in accordance with the number of circumferential rotations they take before reaching the end; first order travelling once around the pipe, second twice etc. In figure 2.1, the ballistic path is depicted with a solid arrow, and the first-order helical paths are depicted with dashed arrows. This way of understanding pipes was used to analyze the helical wave propagation in a pipe in this thesis. This is a common method for analyzing propagation in a pipe structures [18]. Instead of modelling the virtual domains, the calculations were made in single domain with boundary conditions so that the longitudinal edges were connected.

This sort of depiction of the system allows easy calculation of the propagation paths from the wave source to the receiver. The following equation can be used to

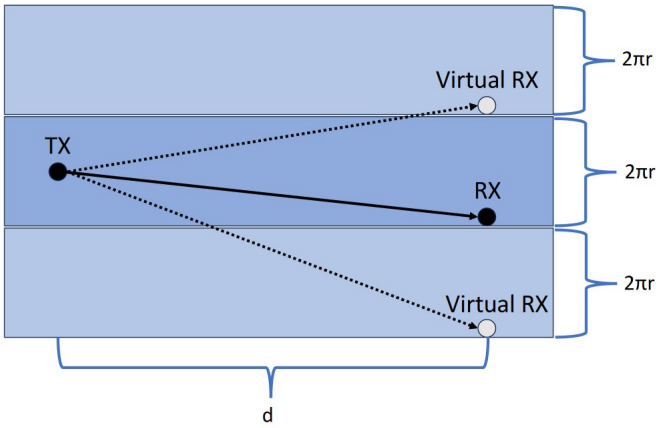


**Figure 2.1:** Actual pipe domain (dark blue) and virtual domains (light blue)

calculate the distance between two units, by understanding just basic trigonometry, from the Pythagorean theorem :

$$d_{RAUS1,RAUS2} = \sqrt{d^2 + ((\theta_1 - \theta_2) \cdot 2\pi r)^2} \tag{2.2}$$

where $d$ is the projection of the distance on the pipe longitudinal axis, $r$ is the pipe radius, and $\theta$ is the circumferential angle between the two units. By adding the helical modes to the equation we get the following periodical distances, if the units are exactly along the same axis or if they are on the opposite sides of the pipe, so if $(\theta_1 - \theta_2) = 0$ or $(\theta_1 - \theta_2) = \pi$, the helical modes will have the distance:

$$d_{RAUS1,RAUS2} = \sqrt{d^2 + ((\theta_1 - \theta_2) \cdot 2\pi r + 2N\pi r)^2} \tag{2.3}$$

where N is the helical mode number that depend on how many times the wave travelled around the pipe. This is just a special case of the system, where clock-wise and counter-clockwise modes travel the same distance. In the general equation, there will be two equations for the waves travelling clockwise (CW) and counter-clockwise (CCW), this is due to the non-symmetrical distances between the units along the paths. The general formula is:

$$1 : d_{RAUS1,RAUS2} = \sqrt{d^2 + ((\theta_1 - \theta_2) \cdot 2\pi r + 2N\pi r)^2}$$
$$2 : d_{RAUS1,RAUS2} = \sqrt{d^2 + ((2\pi - (\theta_1 - \theta_2)) \cdot 2\pi r + 2N\pi r)^2}$$

The shortest helical mode path (1) can either be clock-wise or counter-clock wise, the direction will be governed with the placement of the probes. This can be easily understood by imagining an situation where two probes are placed with a circumferential angle of $\pi/2$ from each other, now the direction of the shortest path is dependent on the direction of the propagation on the longitudinal axis: transmitting from one the

shortest path is either CW or CCW. When the longitudinal propagation distance is reversed i.e. the transmission and reception pair is switched, the shortest path is in the other direction, even though their location relative to each other remained the same.

One can also see from these general equations that the special cases $\theta_1 - \theta_2 = 0$ and $\theta_1 - \theta_2 = \pi$, return the equation for the special case 2.3.

### Wave modes

Lamb waves feature anti-symmetric and symmetric modes. In anti-symmetric mode the wave motion is in opposite phases on the sides of the structure: when the top-layer moves outwards the bottom-layer moves inwards and vice-versa. In symmetric mode the motion is in the same phase on the both sides of the structure: top and bottom layer are moving outwards or inwards when measured at the same distance along the propagation path. These different modes are presented in figure 2.2 by Ensminger and Dale. [19]

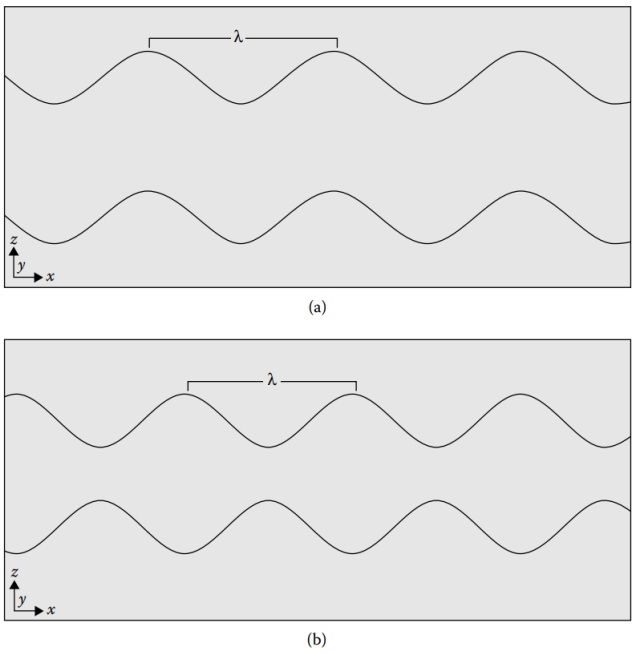


**Figure 2.2:** a) Anti-symmetric and b) Symmetric Lamb mode propagation by Ensminger and Dale [19]

During this thesis two well-known properties of these wave modes are observed: anti-symmetric modes travel generally slower and the displacement measured on the top-layer is greater with anti-symmetric modes. It is also characteristic for Lamb waves that they experience high dispersion, as presented in equation 2.1. This means that the different frequency components of the wave travel at different speeds. This effect is illustrated in dispersion curves. In our case the material was steel, which is very

well studied and both phase velocities and group velocities are readily available in the literature[20]. The velocities of the different Lamb wave modes are illustrated in figure 2.3. During this work, the wave velocities were extracted from the experimental data, and these values were agreeing with the results from the literature. In this case the frequency thickness product was 0.8 MHz*mm, and the group velocity for anti-symmetric mode was 3025 m/s and for the symmetric mode 5100 m/s.

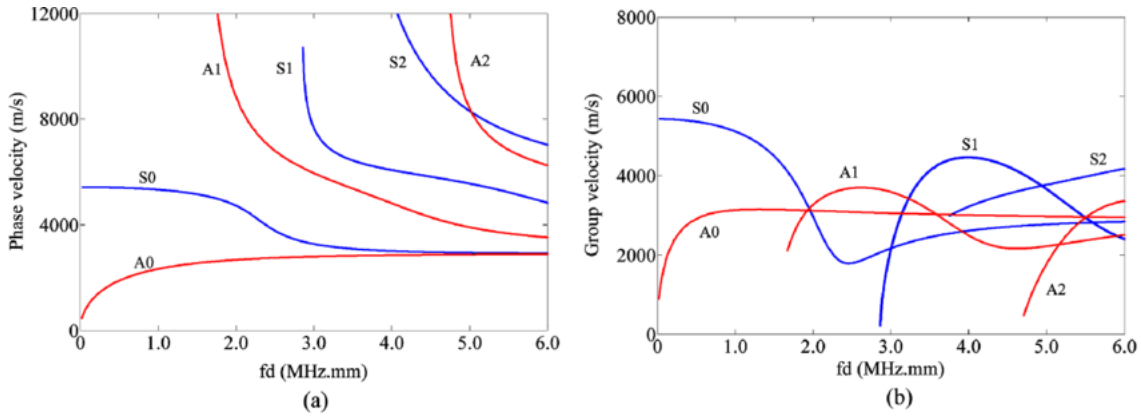


**Figure 2.3:** Dispersion of different Lamb wave modes in steel [20]

The x-axis in the figure describes the frequency thickness ($fd$). For the measurements for this thesis, only the A0 and S0 wave modes were observed due to the low $fd$ in our case. The thickness of the structure was 2 mm and our piezo transducers were operating at 400 kHz central frequency, which gives as a frequency thickness of 0.8 MHz*mm. As represented in figure 2.3, no higher Lamb wave modes can be observed in this frequency in this particular set-up. However, if the devices would be used with a higher central frequency transducers or if the study was carried out in a structure with thicker walls, it would have been possible to use also the higher wave modes for the defect localization. Mathematically speaking, there are infinite amount of higher and higher Lamb wave modes always present when a wave is propagating in a confined structure. Usually in materials testing the lower order, zeroth and first, modes are used, due to the availability of these wave modes in lower frequencies.

The Lamb wave attenuation in flawless media is studied widely in the literature, for example, by Kanji Ono [21]. In this publication, the attenuation was determined for multiple different materials. The attenuation was determined by using wavelet transforms on signals that had propagated different distances. The attenuation was dependent on the frequency and the material where the wave was propagating in. In the work these two rules of thumb were observed for the A0 and S0 Lamb wave attenuation

linking them with the bulk wave attenuation coefficients:

$$\alpha - S_0 \approx \frac{\alpha_L - \alpha_T}{2}$$
$$\alpha - A_0 \approx \alpha_T$$

Here, $\alpha_T$ and $\alpha_L$ are the shear and longitudinal bulk attenuation coefficients, and $\alpha - S_0$ and $\alpha - A_0$ the Lamb wave mode attenuation coefficients. These general equations are well suited in low-attenuation materials, such as steel.

## 2.3 Effects of defects on Lamb Waves

The propagation of Lamb wave will change while it is propagating through the medium due to changes in mechanical properties of the medium, change in loading of the pipe or if the shape of the medium changes. The change in mechanical properties could be for example a weld or a section made from different material than the main body. The change in body loading can be caused for example by fouling deposition on the pipe wall. An example of medium shape change is the most interesting in the context of this thesis; it could be the sudden thinning of the wall (notch) or complete lack of material (a hole in the pipe). The interaction on the defect boundary has been reported for example by Alleyne *et al.* [22]. In their research the key parameter for Lamb wave transmission over a notch is the ratio between the notch depth and plate thickness. The width of the notch does not have a significant effect if the notch width is small compared to the wave length of the propagating wave. They claim that the notch localization is possible when monitoring the frequency change of the modes.

As the structure gets thinner, the frequency thickness product changes which causes the wave to propagate at a different speed. They were performing a two dimensional reciprocal analysis of the wave propagation and displaying the data in frequency and wavenumber maps. This is not possible with the setup used in the experiments carried out for this thesis as the locations of the receivers and transmitters were fixed and the spatial resolution would not yield sufficient resolution in the wavenumber domain as it is the reciprocal of the spatial data; to get a good wavenumber resolution many spatial locations need to be analyzed. The effect of frequency shifting of wave propagation can however be applied in the context of this thesis when using narrow band receivers by a lack of propagating wave or shift in time domain if the propagating wave has passed a notch.

The complete lack of material on the propagating path i.e. when the pipe has a through hole causes more interesting effect than just shift in the signal. The feature caused by the initial wave may completely disappear if the width of the notch and

the angle of propagating wave are so that the wave can not pass through the region. However, the hole creates a new high impedance mismatched boundary: the created steel-air boundary is now perpendicular to the original wave propagation direction. The notches and holes will also cause reflections that travel backwards from the defect.

## 2.4 Generation of Lamb waves

The excitation of guided waves is usually done by either piezoacoustic transducers, electromagnetic acoustic transducers (EMAT)[23] or laser excitation[24]. The excitation with piezoacoustic transducer is possible by applying a voltage difference across the piezo element. The voltage difference will cause strain in the piezo element that causes piezo to deform. This strain is usually converted to a minute displacement on the object which then causes the wave propagation.

The laser based excitation is done by shooting a high power laser pulse at the evaluated surface. The beam will locally heat up the material that causes strain that starts the wave propagation.[25] The profile of the excitation can be adjusted by changing the peak power, color and pulse length. Too high power will cause evaporation of the surface material, this effect is called ablation and is usually not desired as it permanently damages the material. The major benefits of laser ultrasonics is that the probes never need to be coupled mechanically to the structure that is being evaluated and the possibility to adjust the excitation by changing the parameters of the pulse. The drawback of this method is the high price and requirement for eye protection as the laser beams used usually have enough power to cause vision loss. The excitation location must also be clean to have repeatable excitation.

With EMATs the excitation is based on high current flows in circular EMAT coils above the material which cause eddy currents to be induced to the material. The main parameters for the eddy current induction are the conductivity and permeability of the material [26]. Suitability of the EMAT excitation must be investigated for each material, based on these physical properties. In the EMAT sensor, there is also a powerful magnetic field in the probe that will cause Lorentz force on the induced eddy currents at the location where the probe is placed. The Lorentz force will cause the mechanical waves to emerge in the material.

As with the laser based method, there is no need to mechanically touch the surface and the measurement can be done in non-contacting manner. The major drawback with EMATs is their higher price. EMATs also require an exact positioning of the probe above the sample at a fixed distance to have repeatable excitation.

The same three methods can also be used to detect the propagating waves. This is done by means of recording the displacement caused by the waves.

When a piezo acoustic transducer is coupled to a surface and a wave passes under it, the small strain caused by the displacement creates an electric potential across the transducer. This voltage difference can then be amplified and the wave propagation can be recreated from this voltage data in time domain.

The laser based pick-up works on the basis of low power laser beam measurements, for example laser doppler velocimetry (LDV) or laser interferometry. This sort of equipment is very accurate, but also expensive and requires careful alignment of the laser and the sample for the measurements to be repeatable. The laser head used for excitation also requires a lot more power than the pick-up and the different tasks are in most cases done by different laser systems. This drives the cost of the system even higher. The benefits of using laser based method is the ability to perform the evaluation without physically touching the inspected object.

The EMAT system uses the magnetic field to detect the displacement that causes small currents to induce in the EMAT coils. The currents can be converted to recreate the mechanical wave that was propagating.[23]

Because the main goal of this work was to create a system consisting of affordable units to be permanently placed on the pipeline, lasers were ruled out due to their relatively high cost and difficult alignment. EMATs require quite sophisticated driving electronics to be used in both transmission and receiving modes. The piezoacoustic elements were chosen for this project due to the simple nature of using them both to excite the wave and record the displacement caused by waves created by the excitation of the other units. Easily implementable solution for changing from transmission (TX) to the receive (RX) modes was achieved with simple and low-cost field effect transistor (FET) switch circuit.

### Transducer coupling

When using piezo electric transducers for TX and RX, it is very important to make sure that the contact between the probe and the surface stays immutable during the measurements and that the surfaces are properly connceted. Failing to do so will cause various issues e.g. decrease in SNR (signal-to-noise ratio). Generally speaking, the coupling can either be wet coupling, liquid coupling agent between the surface and the probe, or dry coupling, no liquid between the surfaces. Using a liquid couplant for transducer coupling is familiar to most of people from medical ultrasound methods. The couplant is used to ease the transmission of sound between the probe and the object under evaluation. In case of dry coupling the good contact is maintained without liquid layer, this can be achieved for example by tightening the probe to the surface so that it can not move.

The coupling of the transducers to the surface is an interesting topic for permanent assemblies. The coupling must give a tight coupling to the surface, but it must not be too brittle so it can stand vibrations caused by the environment without detaching. In the case of pipes, the vibrations can also be caused by the fluids running through the pipes.

The feasible coupling methods for permanent installation can be divided in clamp coupling, welding and adhesive coupling. All of these coupling methods are dry coupling by their nature. The use of wet coupling could be achieved if the pipe is in immersion, but otherwise maintaining the wet coupling in a permanent installation over months or years is very challenging.

Coupling clamp presses the probe against the surface with a constant force using a device that tightens the unit to the pipe. The clamping device can be either a strap that tightens the device or a metallic clamp that is tightened in place with bolts. For permanent installation a solid metallic clamp should be used. This will give the system moderately good resistivity against vibrations and won't necessarily leave permanent marks on the pipe if it would be ever removed. The drawback of this method is the longer installation time, higher cost and the need for specific clamp for each pipe diameter and shape. Installation to bend sections will also require specific clamps.

When using welding methods, the probe can't usually be directly welded to the surface as the welding process will have temperatures that will damage the piezo element. The transducer should therefore have a front-mass or a delay line that is attached to the piezo element. That additional piece can then be welded to the surface. Alternatively, threads can be used to tighten the probe to the surface if a threaded stub is welded to the pipe. Then the transducer, with a front mass with matching threads, can be screwed in place. This is a common method of attaching high power Langevin transducers in cleaning applications. The benefits when utilizing welding in coupling are the most stable installation. The drawback is the amount of work required as well as the method being limited to pipes that can be welded on.

Adhesive coupling is the simplest method as it has minimal requirements for the pipe geometry and material. There is a wide selection of permanent adhesives for transducer installations available on the market but their properties in vibrating environments needs more investigation. The adhesion coupling was selected for this work due to its simplicity, as the coupling was not the main focus of this thesis.

In the end, the coupling method must be selected on need basis, when there is information about the location and materials where the system is installed.

# 3. Description of the developed system

## 3.1 Overview

The system developed in this project consists of multiple transmission/receiving units, a router and a host computer. A simplified block diagram of a single unit is depicted in figure 3.1.

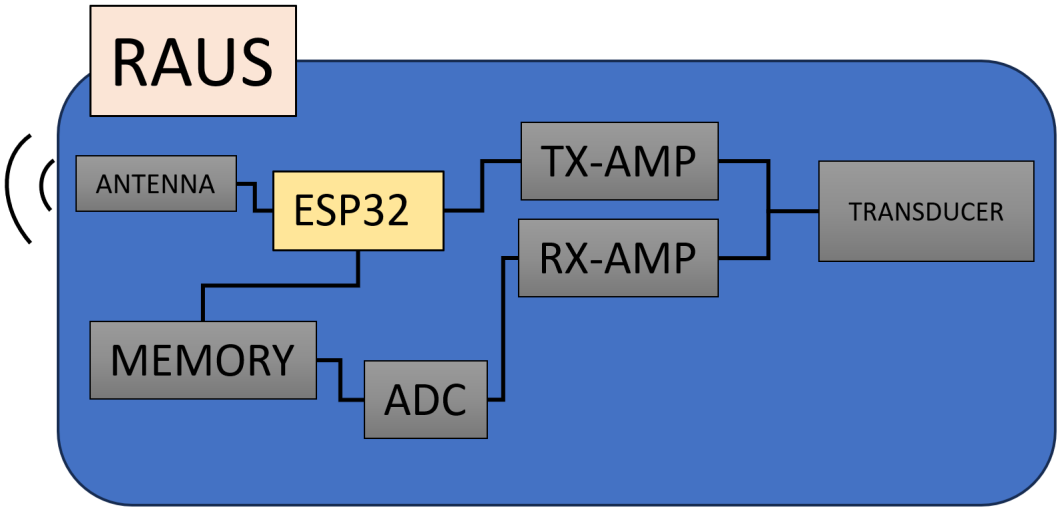


**Figure 3.1:** Block diagram of a single unit

## 3.2 Electronics

The design files for the full project are available upon request from the author. The design was done using KiCAD 5 software. Most of the simple components are found in the built-in libraries of the software. The missing components were created based

on the information provided in the datasheets of the components. The printed circuit board (PCB) design was done as a four-layer board, this saved some time when routing the paths on the board and the manufacturing cost difference between a 2-layer and a 4-layer PCB is not that significant. The electronic design schematic and the board design files are pictured in figures 3.2 and 3.3 respectively. The PCBs were manufactured by JLCPCB (Hong Kong).

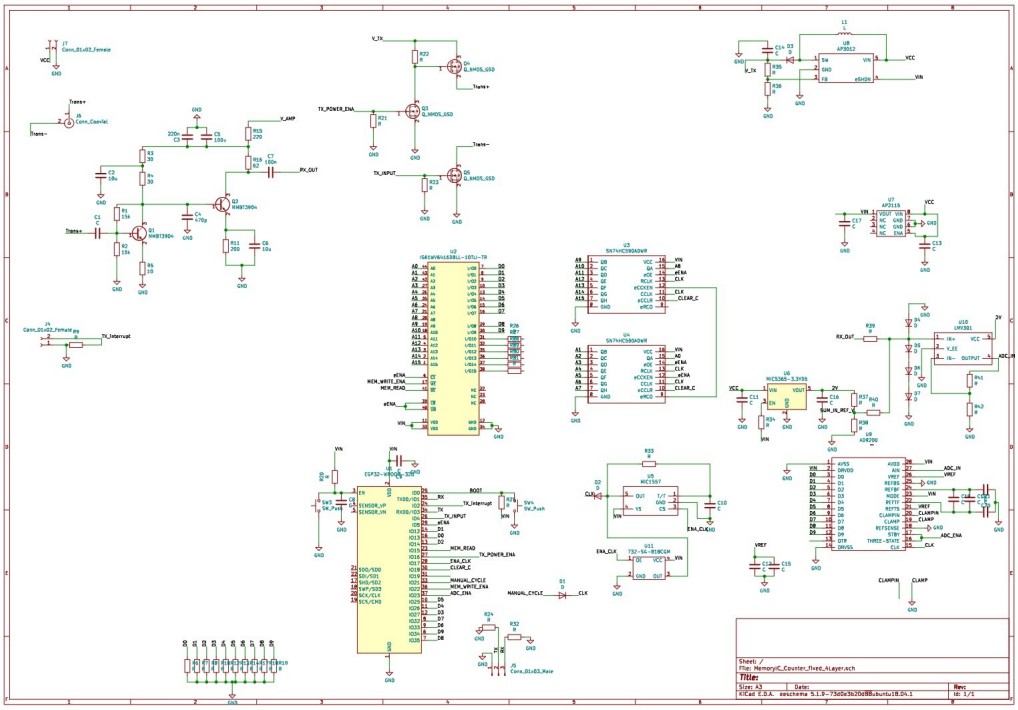

**Figure 3.2:** Schematics of the designed device

It is pretty difficult to show in image format the design of a multilayered PCB. The separate layers can be found in the appendices.

Multiple iterations of the PCBs were made during the testing phase. The version of the PCB, which was used during the measurements of this work, is presented in figure 3.4. As is obvious from the figure, some modifications had to be made on the board to make it work properly. The changes have been updated to the design files and are visible in the most recent version available upon request.

### 3.2.1 ESP32

ESP32 by Espressif was selected as the microcontroller due to its low price, low power consumption and easy to implement libraries for the use of WiFi-interface. This device acts as the access point for the wireless network and the main instructor for the other components. There are several different modules that utilize the ESP32 chip. From

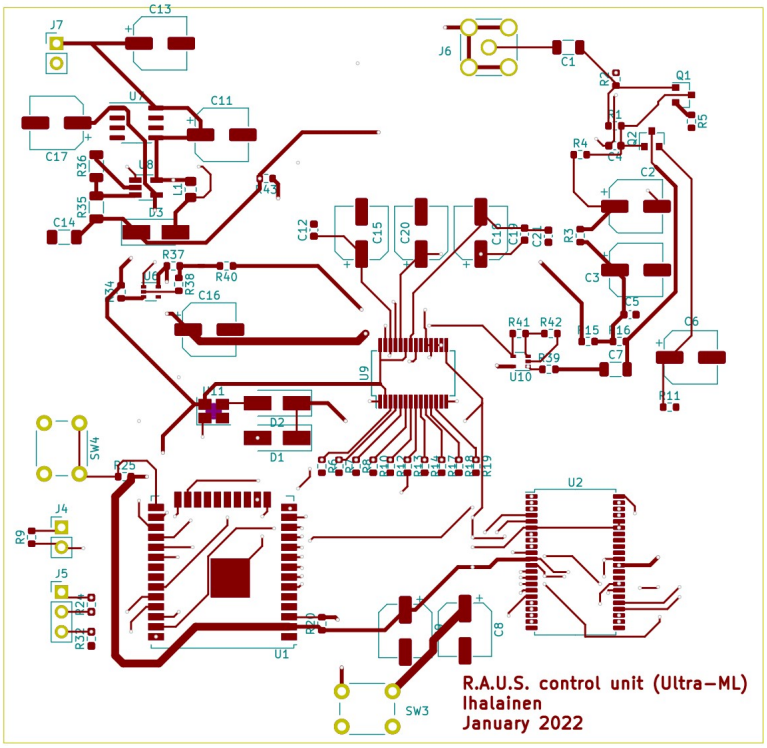


**Figure 3.3:** Top layer of the PCB design without the ground plane fill

these, the ESP32-WROOM-32E was selected due to good capabilities, affordable price and good availability. The selected model also came with a on module antenna so the connection to the router was reliable and stable without making a custom antenna on the PCB. Programming of the ESP32-WROOM module was done by using the Arduino IDE environment. Suitable compiler is available in the ESP32-library; the Firebeetle board compiler configuration enables the compilation and uploading of the firmware to the chip. The universal asynchronous receiver transmitter (UART) line was used to upload the firmware to the device. A simple USB-UART converter was used to connect the programming computer to the TX/RX pins of the UART port on the device. This converter was not included to the design, but used as an external tool.

Even though ESP32 is a quite powerful micro controller, its built-in analog-to-digital (ADC) modules are not fast enough to record ultrasonic signals in our case. The internal ADC sampling rate of ESP32 is 200 kSps when used in real-time clock (RTC) mode. The sampling rate can go as high as 2 MSps if used in DIG mode. [27]. The central frequencies of the transducers that were used were around 400 kHz. The sampling rate of the ESP32 would not be able to capture the signals accurately in the time domain. So, a separate ADC module was used. The selected model was AD9200 by Analog devices, it is capable of doing analog-to-digital conversions at a maximum rate of 20 MSps with 10-bit resolution. This is high enough to record the signals in the 400 kHz range or even higher frequencies if a different probe is used.

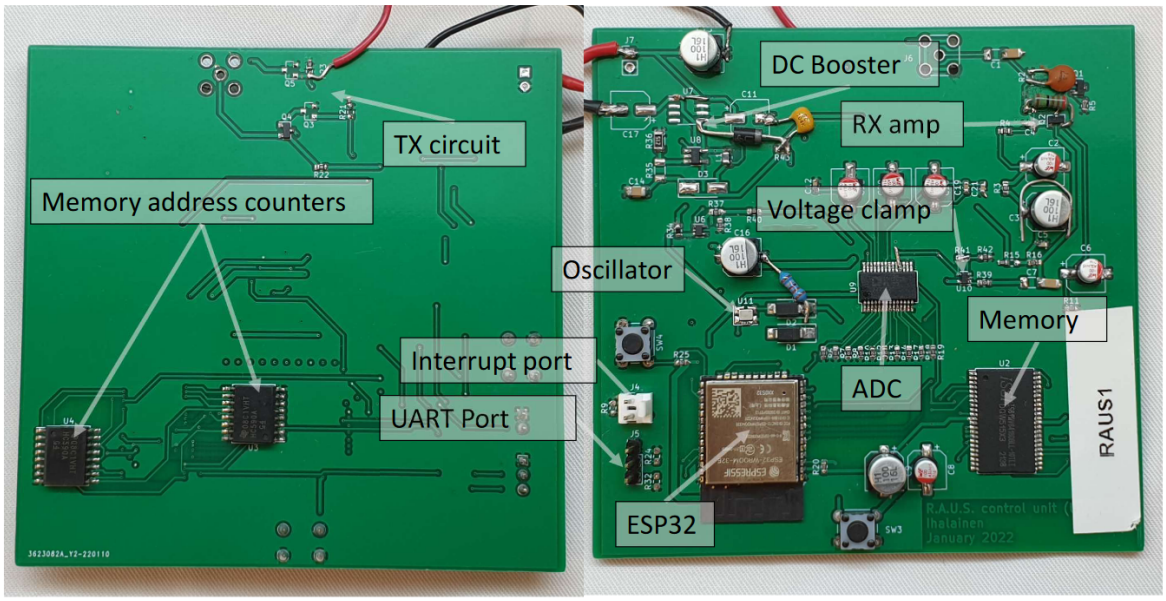


**Figure 3.4:** Assembled PCB, Left: Bottom side, right: Top side, photo by Julius Korsimaa

Too low sampling rate will result in aliasing of the signal. This means that the sampling frequency will not be able to capture the features with higher frequency. Nyquist's theorem states that the sampling frequency can not capture frequencies that are higher than half of the sampling frequency. Explicitly the theorem states, that no higher frequency components can be reconstructed from the signal that are over half of the sampling frequency. The effect of aliasing with different sampling frequencies is presented in figure 3.5. The reconstruction will become much harder when there are multiple frequencies overlapping.

### 3.2.2 Digitizing the signal

The ADC provided the conversion as a parallel output from 10 different pins. ESP32 is not fast enough to record the output straight from the ADC, so a memory integrated circuit was deployed. A fast 16 x 64K memory module was used for this, namely IS61WV6416DBLL by Integrated Silicon Solution Inc. The size markings mean that the module can hold 65536 16-bit samples. Only 10 of the bits were needed for the ADC output, but due to common needs in the industry, 16-bit memories are produced in larger quantities than 10-bit, which are quite rare. This also leaves head-room if a higher resolution is needed or if some meta data needs to be stored in the future. The writing address was controlled with two 8-bit counters, namely SN74HC590A by Texas Instruments. The counters were in cascading configuration; Only one of the registers was connected with the system clock signal. When the lower counter reaches the maximum value of 255 (11111111) the next rising edge from the system clock

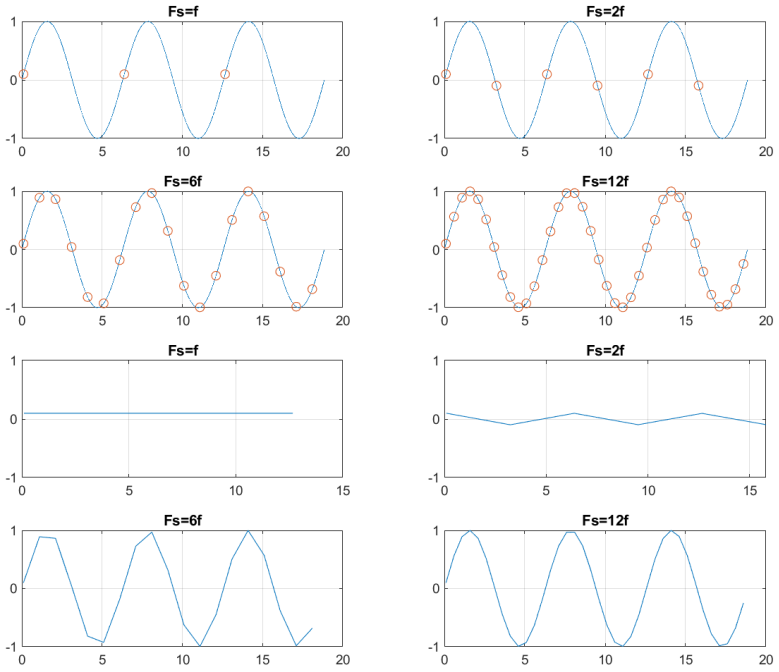


**Figure 3.5:** Top: sampling points on a single frequency sine wave with different sampling rates, bottom: reconstructed signals based on the samples

overflows the lower counter setting it back to value 0. The overflowing signal from the lower counter is used as a clock signal to forward the upper register by one step. This sets the combined register value to (00000001)(00000000)=256. The lower counter therefore acts as the bits 0-7 and the upper register as bits 8-15. These counters dictate to which address the ADC value is written to on the memory chip. This configuration is explained more in the datasheet [28]. Only one oscillation signal was needed for the device; the same rising edge told ADC that it was time to output new reading, memory IC to save the reading to the current address and the counters to change the address for the next reading. The system clock signal for the procedure was created with a separate 4 MHz crystal oscillator. If a higher or lower sampling rate is required, the oscillator can be swapped out to any oscillator up to 20 MHz, as the ADC module is limiting the maximum conversion rate. A simplified illustration of the digitization and data saving is presented in figure 3.6.

### 3.2.3 Writing procedure

Writing procedure starts when the ESP32 receives the interrupt signal from an other unit. This starts an interrupt function that stops the current execution of the loop()-function. In the interrupt function ESP32 enables ADC by pulling I/O 23 low, this

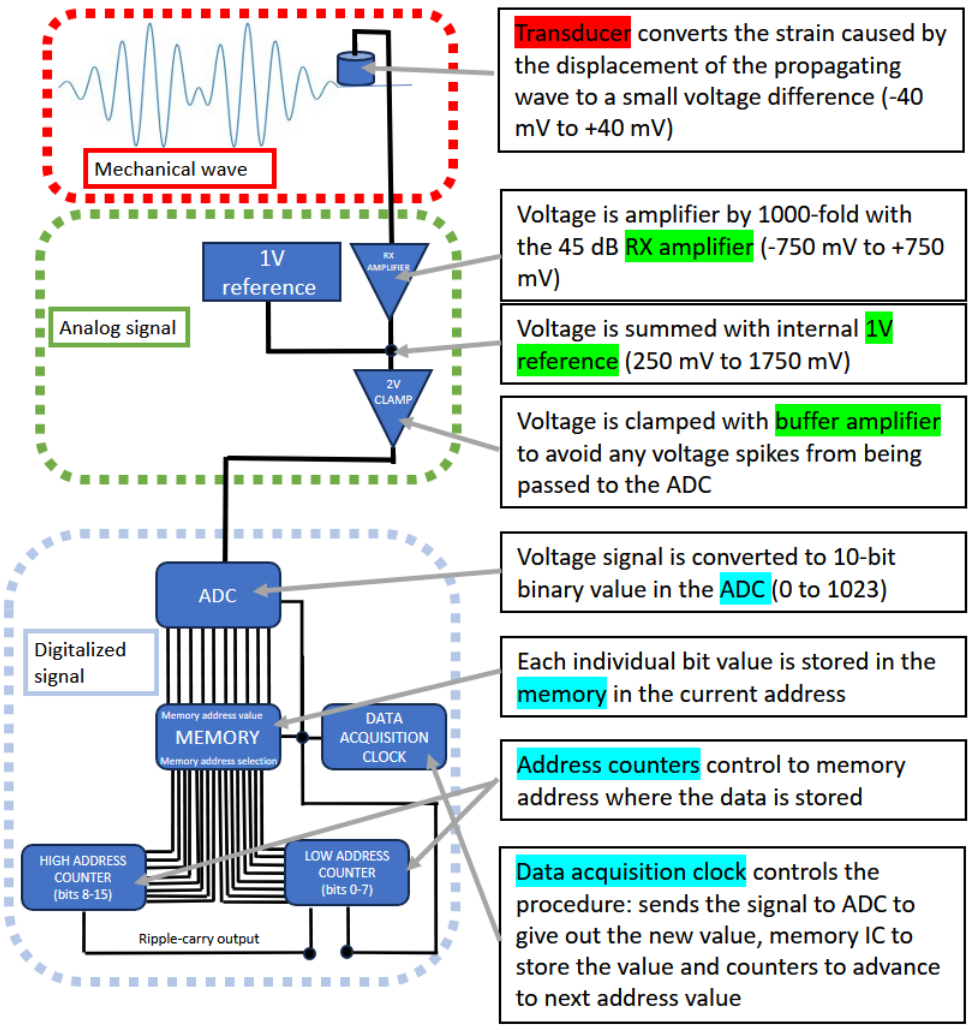


**Figure 3.6:** Simplified illustration of the digitization process

activates the ADC to write and to pass readings from the internal buffer to the parallel output. Then the clock IC is disabled so the counter ICs can be reset, this happens by pulling ESP I/O 17 pin low. The resetting happens by pulling CCLR pin down, cycling the clock signal by one step to clear the counter and then resetting the counters. Then the external crystal oscillator is enabled which starts the synchronized operation between the ADC, memory and address counters and the digitized signals start to fill the memory addresses.

### 3.2.4 Reading procedure

After the measurement is completed, ESP32 reads the data from the memory IC and relays it to the host device. ESP32 goes trough the addresses by providing a square wave signal that mimics the oscillator signal to access the memory locations but with

| function | low-side FET | high-side FET |
|---|---|---|
| RX | open | closed |
| TX | input signal | open |

**Table 3.1:** The control states of the RX/TX circuit

a lower frequency. ESP32 accesses the data stored in the memory IC for the amount of addresses that there is data, this is determined by the clock frequency and the data acquisition time. The memory IC will give the saved binary values as they were given by the ADC IC, as a parallel output. In retrospect, a parallel in-serial out (PISO) shift register or a multiplexer could have been used to access the data with ESP32 using single data pin. Also there would have been an option to add a serializing IC to the parallel data lines. However, because there was enough digital data pins available on ESP32, the data was easy enough to get from the memory by connecting the memory outputs to the ESP32 inputs.

## 3.3 Piezoacoustic transducers

Piezoacoustic transducers are devices capable of transforming electric signals into strain. They can also convert strain difference into potential difference between the transducer terminals. This strain can be translated into displacement when the device is coupled to the object that is being evaluated. Here the actions for RX and TX are examined for one single unit. The switch circuit that changes the state of the device between transmission and reception is illustrated in figure 3.7. The transducer is connected to the PCB to a circuitry that consists of a high-side N-type field effect transistor (NFET) (Q4 in the figure) and a low-side NFET (Q5 in the figure). The high-side switch controls whether the transducer is in TX mode ( drive voltage at the piezo positive terminal) or in RX mode (piezo positive terminal is floating). The low-side switch controls the negative terminal of the transducer. In TX mode it is used to create the actuation signal by switching the negative terminal to ground and floating it. In RX mode the negative terminal is grounded. The controls of the NFET switch are displayed in Table 3.1.

When the unit is in transmission mode, the driving FET (Q3 in the figure) can be used to drive the piezo element. This is done by giving a train of pulses from the ESP to the gate of the driving FET. In this work a burst of four square waves at 50 % duty cycle and 400 kHz frequency was used. In later iterations of the system, the duty cycle and pulse count are adjustable.

Round circular piezo elements with a central frequency of 400 kHz and diameter

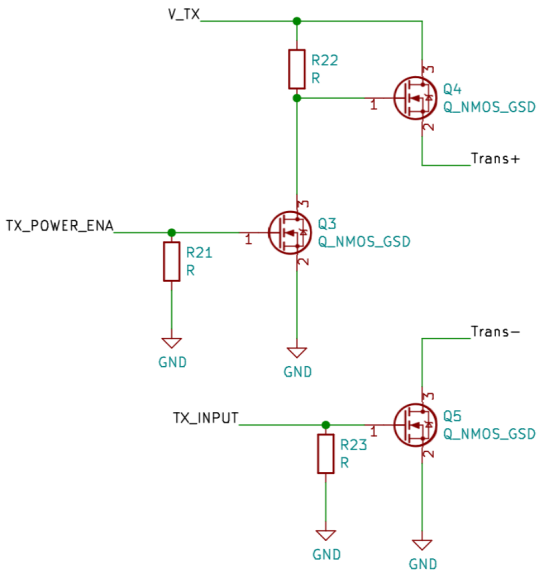


**Figure 3.7:** NFET control circuit

of 5 mm were used as transducers in this study. These components were procured by StemmInc (product ID: SMD05T04R411). Piezo discs were connected to 1 mm thick glass plates that isolated them from the pipe. The possibility of adding piezo backing behind the elements to widen the bandwidth was investigated. However due to difficulties on preparing the backing consistently to multiple transducers, the piezo elements were used without any backing. Non-backed piezo elements have the highest sensitivity at the resonance frequency, but are very prone to ring [29].

### 3.3.1 Receiving mode

In receiving mode the drive voltage is disconnected by opening the high-side FET. The propagating wave on the pipe will cause time-dependent displacement on the pipe under the transducer. This displacement causes strain to the transducer which causes electric potential between the positive and negative terminal. The negative terminal is grounded through the open low-side FET and therefore the potential on the positive terminal is relative to the ground. The small voltage change caused by the propagating wave is then amplified by the bipolar junction transistor(BJT)-amplifier. Amplified signal is then biased and amplified by the fixed 2 gain non-inverting amplifier. This signal is then fed to the ADC which digitizes it.

### BJT amplifier

Due to the low amplitude of the received signal a large gain was needed before digitization. While searching for an amplifier for low amplitude input signal amplification, two key elements were considered: gain-bandwidth product (GBP) and phase shift.

GBP describes what is the maximum gain as a function of the frequency. The unit of GBP is in hertz because the gain is a dimensionless parameter. For example an amplifier with GBP of 4 MHz will be capable of unity gain at 4 MHz. When the amplifier is configured to operate at 10 times gain, the maximum frequency it can operate is 400 kHz (10*400 kHz=4 MHz).

Phase shift describes how the phase of the input signal is affected as a function of the frequency of the signal. Around 40 dB gain was considered to be sufficient to utilize the whole 2 V scale of the ADC. For signal with a frequency of 300 kHz this means a GBP of 12 MHz. This is something that can be done with current single packet amplifiers, however the phase shift for these IC's is usually not good for wideband applications. This means that the phase of the output signal will change depending on the frequency components of the signal. This can be a problem if the electronics are used with a more wide band transducer. The signals can be adjusted in post-processing by applying the information about the phase shift to the output signal. However a simpler solution is to make a custom amplifying circuit. This also proved to be a meaningful task in the frame of this work. By designing a custom transistor amplifier, both high gain and minimal phase shift in band was accomplished. Using a custom circuit is much more affordable than using a ready off-the-shelf IC. Design work was assisted by using a circuit simulator tool, which was LtSpice by Linear Technology. The designed circuit did have amplification of 45 dB in the band with small phase shift (20 degrees) from 100 kHz to 1 MHz. The final circuit design and LtSpice simulation with the output amplification and phase shift are presented in figure 3.8.

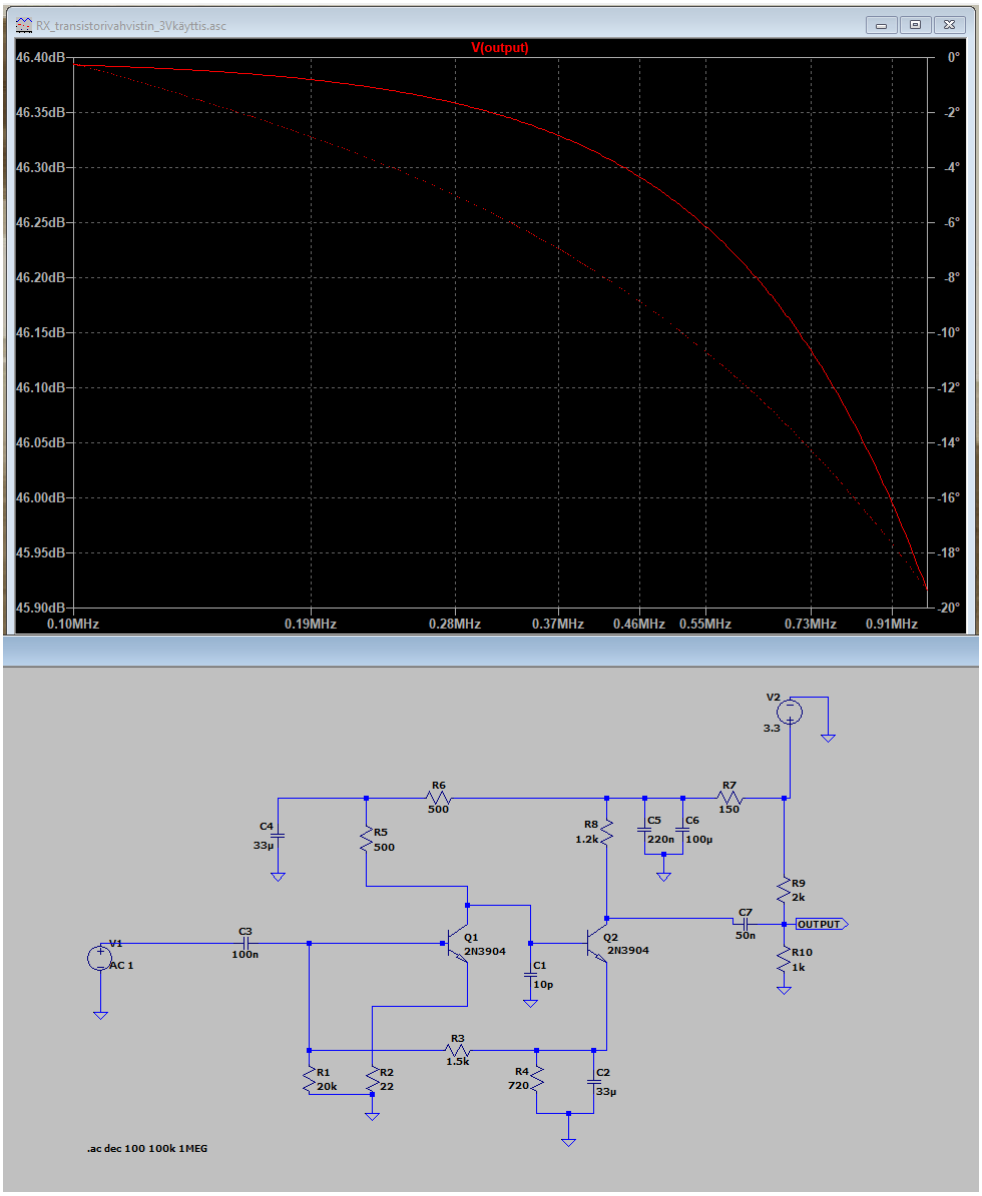


**Figure 3.8:** Amplification and phase shift of the RX amplifier simulated with LtSpice using small signal AC analysis tool

### 3.3.2 Transmission mode

In transmission mode the high-side switch connects the positive terminal of the transducer to drive voltage of 27 volts. The low-side switch is then used to control the electric field across the piezo element. By pulling the FET gate to logic high voltage, the FET opens and electric field exists between the terminals causing strain which then translates to a local stress on the pipe. Then by pulling the gate to low voltage closes the FET and the transducer returns to the base state removing the stress from the pipe. The stress changes on the steel pipe launch propagating waves in all directions from the transducer. The transducers could therefore be considered as point-sources when operating in transmission mode. Due to coupling to the pipe the excitation was more close to a line-source.

## 3.4 Networking

A software for the client was created to control the devices on the network. Graphical user interface (GUI) was developed for the user convenience. The software was programmed by using the python tkinter library. The simple GUI is shown in figure 3.9. To connect the devices to the client computer, client computer must join the

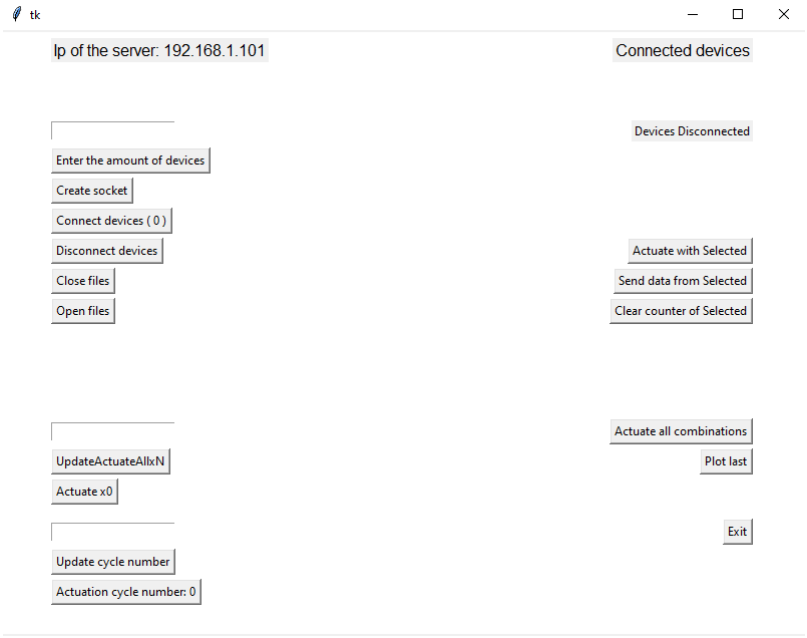


**Figure 3.9:** An overview of the GUI

local area network (LAN) where the devices are programmed to connect on boot-up. During the measurements, an external router was used to host the network. The ESP boards search the LAN to find the client computer by using a Domain name system

(DNS) list for host devices. The DNS list of possible client computers was stored to the firmware of the devices. When the ESP32 finds the DNS by name, it gets the IP-address of the client and connects to that IP. Then the ESP waits for the operation it needs to perform; should it prepare to actuate on the pipe, prepare to record the signal to its memory or send the data from the memory to the client. The communication was made using WiFiClient-library on the RAUS side and python WiFi-library on the client computer side.

The delay with the used libraries and implementation was not constant, when operating over Wi-FI. This is not a problem when using the non-time critical tasks, such as sending the stored data from the RAUS unit to the client. However this is an issue, when the time critical operations must be performed, such as informing the other devices that a signal is being actuated and must be recorded by them. The latency variation makes it impossible to precisely and repeatably start the recording the signal. The time window for one measurement in this use case was just 1 ms. This meant that the possible wireless jitter of up to 500 ms, which was observed, was unacceptable. Due to difficulties of synchronizing commands on wireless network in TCP/IP protocol with the used libraries, a wired trigger line was deployed between the units to ensure that the TOFs are accurate depiction of the propagation time of the guided wave. In the literature there are ways to synchronize wireless devices down to sub microsecond range with minimal jitter by using the User Datagram Protocol (UDP)[30], however wired connection between the devices for triggering was settled on in the frame of this work. Accurate triggering was accomplished by using an interrupt pin. A function attached to an interrupt pin will stop the current action on the device and start the recording function as soon as possible. The jitter caused by this method was in the order of tens of microseconds.

In later iteration of the system, the physical interrupt line between the units has been replaced with a wireless trigger.

# 4. Experimental results

## 4.1 Set-up

A stainless steel (AISI 304) pipe was used to test the defect detection with the system. The pipe was 253 mm long, 154 mm in diameter and the wall thickness was 2 mm. 5 RAUS units were placed on the pipe with 300 mm separation along longitudinal axis and 90 degree along the pipe circumference, the locations are illustrated in an unwrapped pipe wall in figure 4.1.

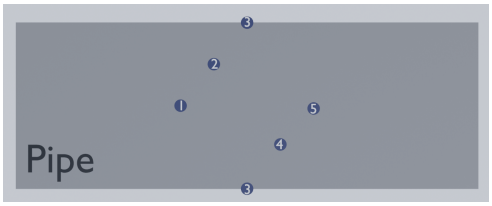


**Figure 4.1:** Locations of the five units on the unwrapped pipe (RAUS units are not to scale)

First the signals on the unaltered pipe were measured between all of the RAUS units. Then a high RPM multitool (Dremel 8820) with a steel cutting disc (Dremel SC456) was used to damage the pipe wall. The damaging was made in 7 steps, from slight damage on the pipe wall all the way to a through hole. The damage is located on the same cicumferential location as RAUS 4 and axially between RAUS 2 and 3. The location is illustrated in figure 4.2. The different levels of damage are illustrated in figure 4.3. Because the damage should cause a difference in the detected waveform only if it is between the transmitter and receiver, some pairs should not detect any changes during measurement. e.g. pair 1-2 and 4-5 should keep the same signal during the measurements. These are important references to make sure that cutting the pipe will not affect the coupling of the transducers.

## 4.2 Results

A training set of defects is required to train the algorithm, which can then localize the unknown defect location by comparing it to the training set. For example in the

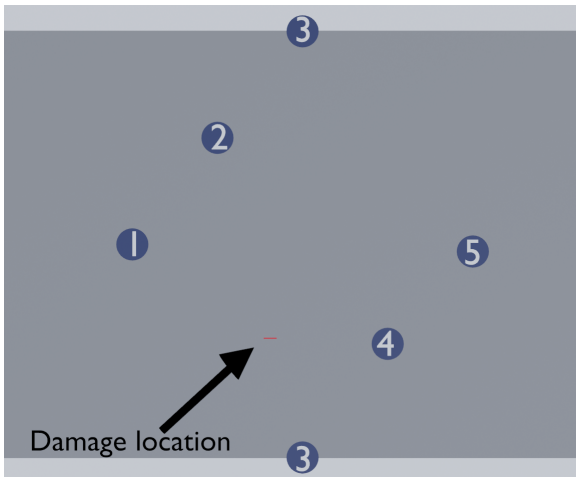


**Figure 4.2:** Location of the damage on the pipe

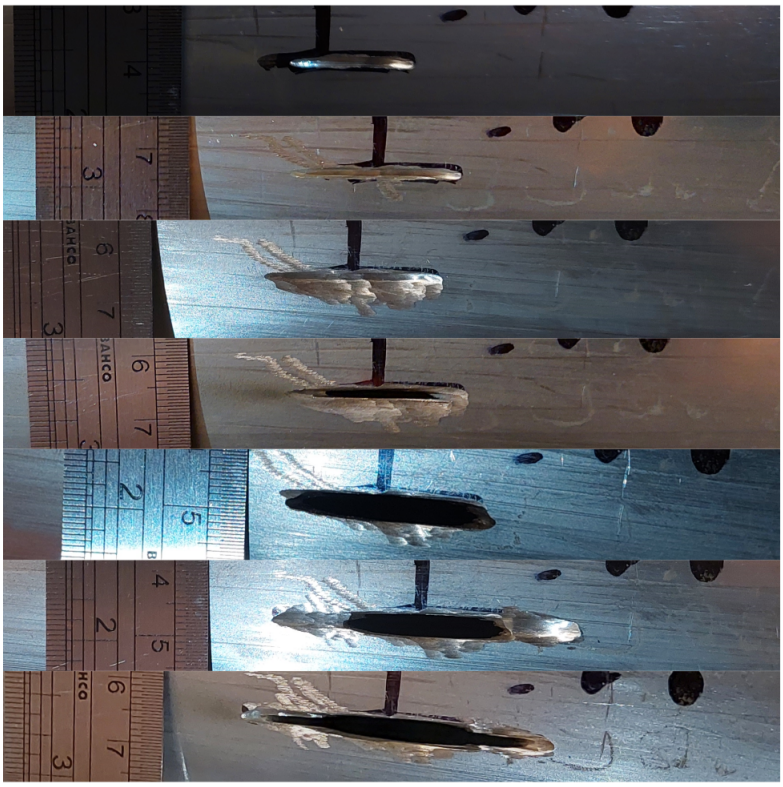

**Figure 4.3:** Level of the damage in the different measurements

paper by Golato *et al.* [31], the training was done by dividing the region of interest with a grid and placing a sample on each of the grid locations. After the training the system was able to determine with relatively high reliability the unknown location of the fouling.

In this thesis the location of the defect is confirmed by looking at the paths which change when the defect gets bigger after the grinding. To give an example on

the recorded signals, two different signals are represented in figure 4.5. The signals here are recorded using RAUS 4 and transmitted with RAUS 2. First example is from the unaltered pipe and the other from a pipe that has the most damage to it: There seems

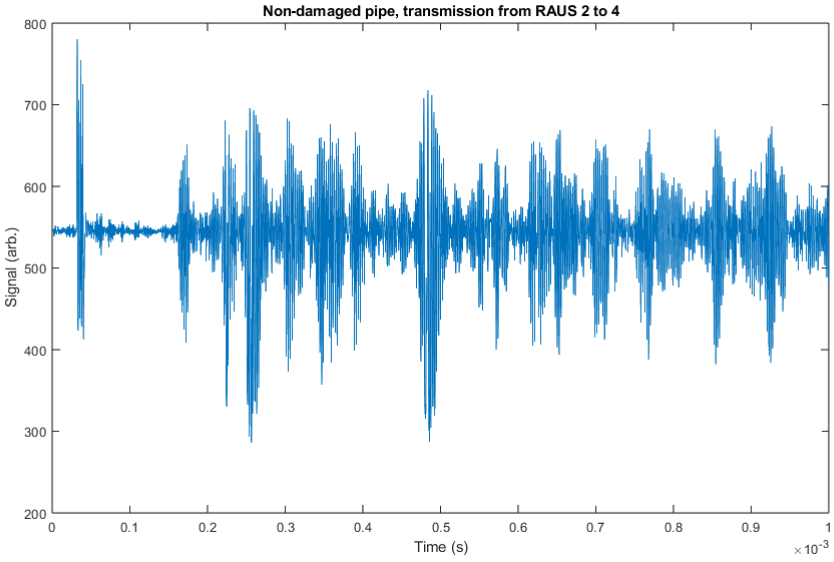


**Figure 4.4:** Unaltered pipe

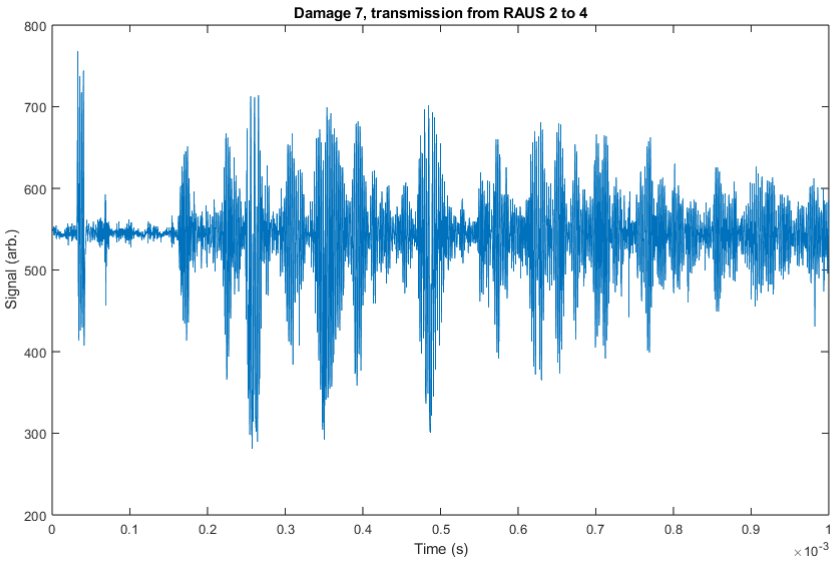


**Figure 4.5:** Damage 7 pipe

to be some alterations in the signal; But to localize the defect better, more careful analysis on the difference between the two signals is required. As stated in the theory section, the localization is based on attenuation and reflection of the travelling wave mode. So if the path is altered in any way, the arrival time will shift, or new peaks will emerge from the reflected waves arriving to the receiver.

This is the method used in this work to find the helical paths which contain

differences when the pipe is defected. Now we can overlay the differential signal of the said RAUS couple to highlight this effect of the signal alteration and shift 4.6. This gives us the arrival times of the different modes. From here we can backtrack to

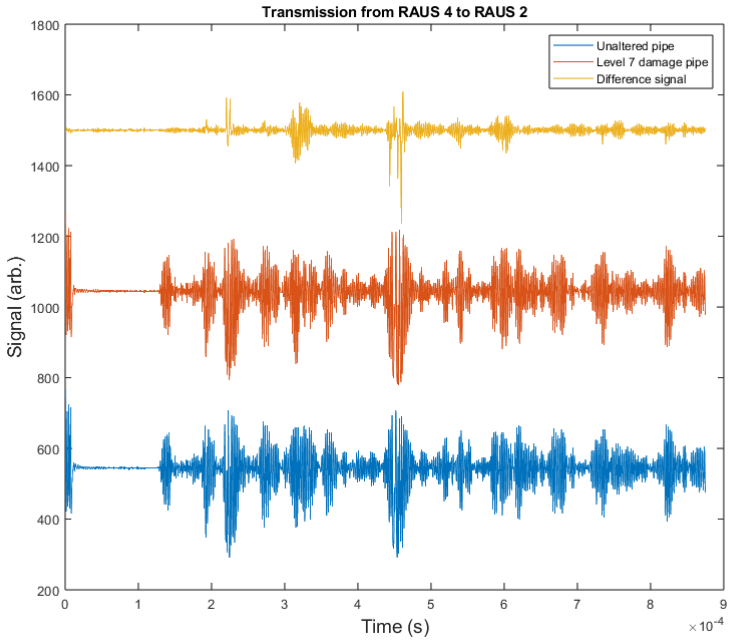


**Figure 4.6:** Differential signal

calculate the distance wave would have to travel between the two units to take this amount of time. Now we have to keep in mind the possibility of the wave to travel along the pipe surface either clockwise and counter-clockwise, as stated in theory section. As can be seen from the data, the signals do not arrive as easily detectable single packets, but there is a lot of overlap in the signals, and also some ringing as mentioned in the theory section. This is caused by the multitude of anti-symmetric and symmetric wave modes travelling both clock-wise and counter clock-wise in a relatively small domain.

The effect of the defect formation is most easily seen by compiling a figure which show the difference signal between the unaltered pipe and the signal for each of the different levels of damage. The compilation is shown in figure 4.7. As one can see from the figure the most dramatic differences are recorded with the pairs which have the defect between them. Then again pairs 1-2 for example seem very flat over the whole range; the defect located not between them has minimal effect on the transmitted and received signal. Also the graphs are symmetric along the diagonal, which gives a good confidence about the units being similar to each other. The individual signals of the units may wary a bit, but the difference signals seem to agree between them.

However, some curious effect can be seen with the transducer pair 3-4, there the signal goes up with the defect depth even if the defect is not located between

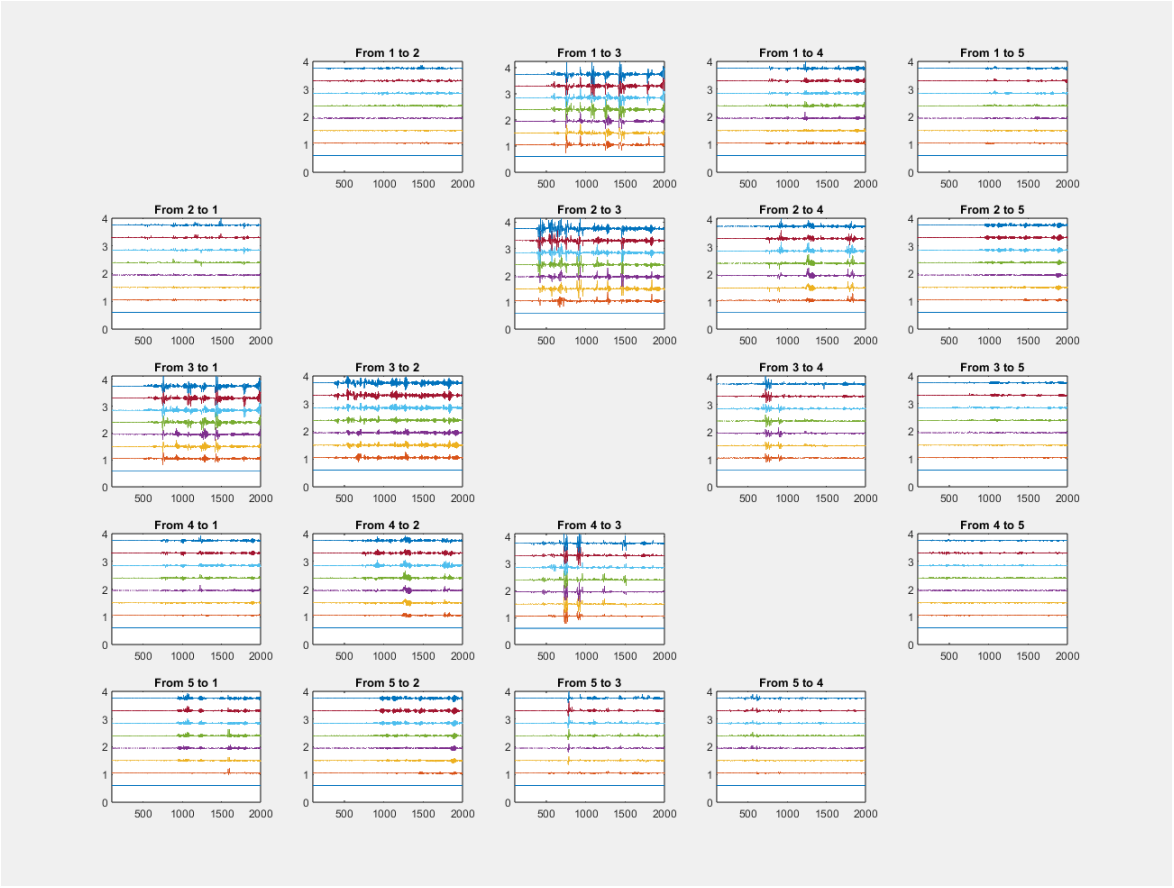


**Figure 4.7:** Differential signals of the received signals between each of the RAUS pairs, the defect severity goes up in the graphs

them. This is most likely the wave being reflected "backwards", but this needs further evaluation. In the previous studies, where instead of defects, solid pieces of fouling were localized using the system the effect of reflection was rarely observed [32]. Instead the localization could be done by tracking the attenuation of the helical modes. The addition of reflection added complexity, when determining how to extract the location information from this data set.

### 4.2.1 Localization

A simple algorithm was made to represent the localization capability of the system from the collected data set. First a peak detection algorithm was programmed. it was applied to the difference signal data, example in figure 4.6. The algorithm was able to determine the time of flights for the paths with differing signals. This information could then be used backwards to calculate the path length which corresponds with the arrival time of the detected difference. Here we have to assume the group velocity of the signal to do this. We can use the arrival times of the signals in the non defected

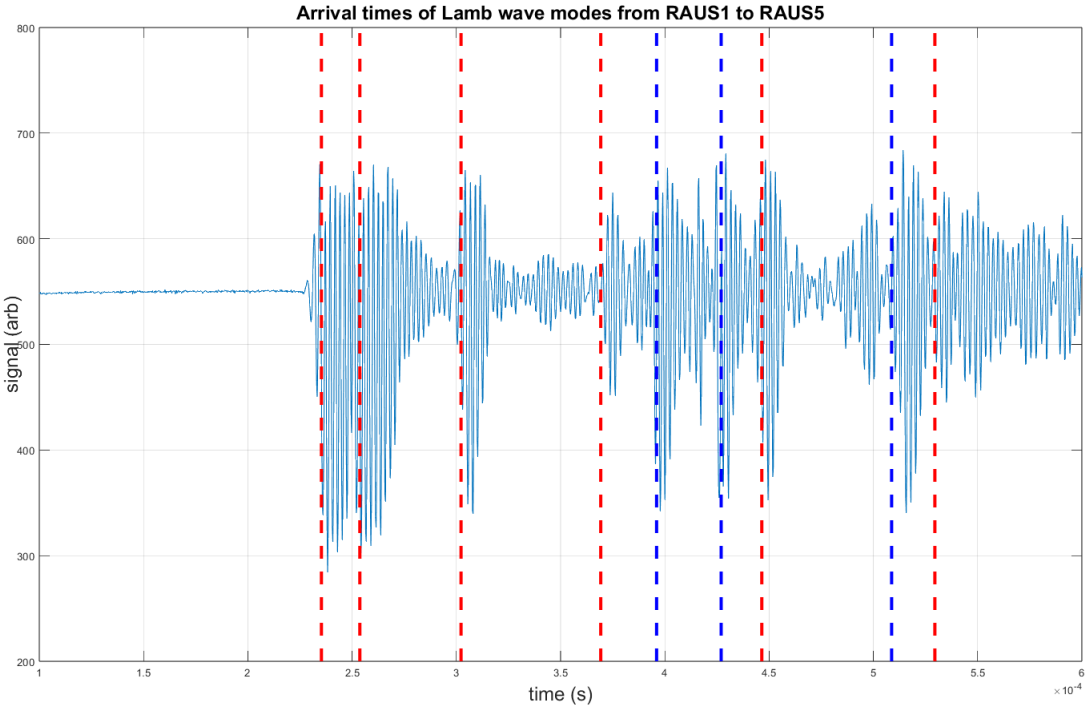


**Figure 4.8:** Signal from RAUS1 to RAUS5 with overlay of the arrival times of symmetric (red) and antisymmetric (blue) wave modes, with speeds of 5100 m/s and 3025 m/s, respectively. The first line is the ballistic signal (i.e. zeroth order helical path)

pipe to calculate the arrival time of the modes.

The following speeds for the modes were calculated from the arrival times: 3025 m/s and 5100 m/s for the antisymmtric and symmetric mode respectively. The arrival times for the helical modes between RAUS pair 1 and 5 is pictured in figure 4.8. This pair was selected because they lie on the same circumferential coordinate and the number of helical paths is thus halved. The symmetric mode is captured very well by the system. The values for the propagation speeds agree with the literature. Once the path lengths were resolved with the peak detection algorithm, the path vectors were given to a simple brute force algorithm that solved the possible paths the wave could have taken between the transmitting and receiving unit to arrive with the detected time. The working principle was the following: A domain is created to represent the space of an unrolled pipe surface, all of the coordinates of the units were defined by their circumferential and axial coordinate.

The domain was split into 1 mm2 sections, therefore the domain had dimensions of 483x1200, circumference of $\pi * 154mm \approx 483$ mm, and 1200 mm length. Then each transducer pair was analysed in nested loops, this was done by starting drawing paths from the first transmitter, for each helical mode and direction. Each simulated

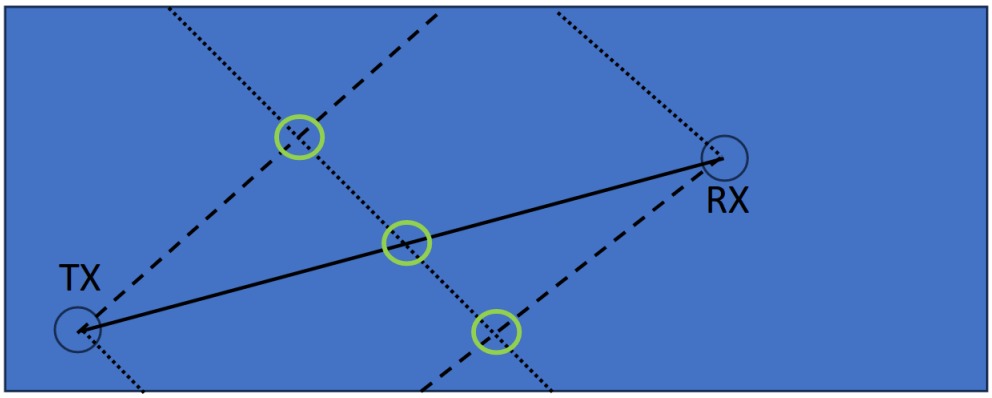


**Figure 4.9:** A simple illustration of the localization algorithm

propagation started by adding the starting coordinates to a 2-dimensional matrix. If the wave would ever leave the domain from the circumferential axis, the crossing coordinates were added to the matrix. The helical mode was given by calculating the ratio between the circumferential and axial components. The axial step was kept at 1 during the propagation, the angle was achieved by altering the circumferential step in relation to the axial step.

When the wave reached the axial coordinate of the receiving transducer, the circumferential coordinate was compared against the circumferential coordinate of the receiver, to determine if this wave could be recorded by the receiving transducer. The distance travelled by the wave was also kept track of. This distance was compared in the end against the possible path lengths given by the peak detection algorithm. If the wave was in suitable position for the receiving transducer to detect it, and the path length agreed with one of the possible path lengths, the path coordinates were added to the list which kept track of all of the suitable paths. A simple illustration of the detection is given in figure 4.9, with one transmitter and one receiver unit. In this case there are 3 paths which cross, giving us 3 similarly equal points for the defect to be.

By increasing the transmission-receiver pairs, and the helical paths, the algorithm will find more paths and the crossing points around areas that are more likely to contain the defect will be represented by more crossings. This method will never be absolutely certain about the exact location, but can find areas that are more likely affected. This proved to be the best method to visualize the otherwise very convoluted data set.

The whole simulation consisted of running 50 wave packets for first 8 helical paths, both clock wise and counter clock wise for each of the 5 transducer pairs. So the final result matrix was a sum of 50*10*2*4*4=8000 paths. As the simulation was very simple to run, it took around 15 to 20 seconds to run this on a desktop computer (Ryzen 3700 with 32 GB RAM) . More exhaustive search could have been made by

increasing the number of wave packets for each test, increasing the number of helical modes would not increase the number of good paths, due to the time limitation of the recorded signal length. Even if there would be higher order helical modes, those would not be captured by the device and so they could not be linked to the experimental data. It was clear that the A0-modes gave a better approximation of the damage location, as there is more time between the arriving waves, giving fewer false positives than when using the S0-waves for the localization.

An additional "reflection coefficient" parameter was added to the simulation; the simulated wave had a small change to "reflect" during the propagation, this was done by flipping the circumferential velocity. This addition was necessary because the data was very convoluted with the different wave modes and signals reflecting from the defect. The requirement to see the reflections also motivates using such a complex method to find suitable paths instead of just straight calculating mathematically which paths are seen in the difference signal. The used reflection method did not flip the axial velocity, so it did not accommodate for the "backwards" reflection. The possible paths matching with the measurement data for all of the seven damage depths is displayed in figure 4.10.

The location of the defect can be illustrated by displaying the points where the lines cross, those are the crossing points of the paths that "saw" the difference. The crossing point are an easy method to investigate where the defect is most likely located, it is not a perfect method but guides the focus on certain points based on the following idea: if we see a lot of differences in the paths crossing the same area on the pipe wall, probably there is something defective in that location. The crossing points were found from the path lines by using an "interX"-algorithm by NS [33]. These points were then added to a matrix with the dimensions of the original domain and the matrix was normalized. The resulting domain then represents the probability for the location of the defect on the pipe according to this algorithm. The crossing points for the damage depths with the actual damage location is displayed in figure 4.11.

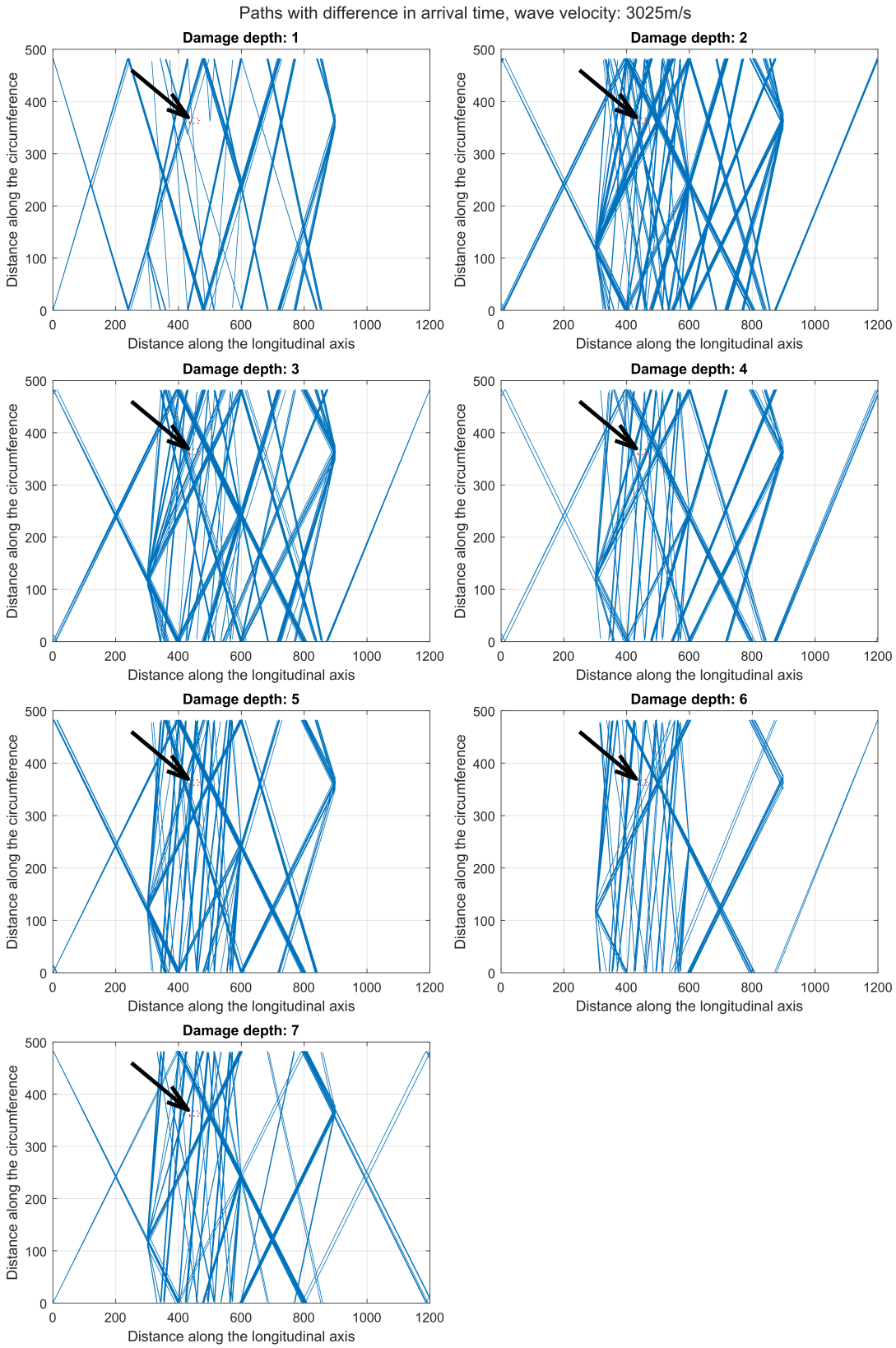


**Figure 4.10:** Paths with difference in arrival time, the location of the defect is marked with red rectangle pointed with black arrow

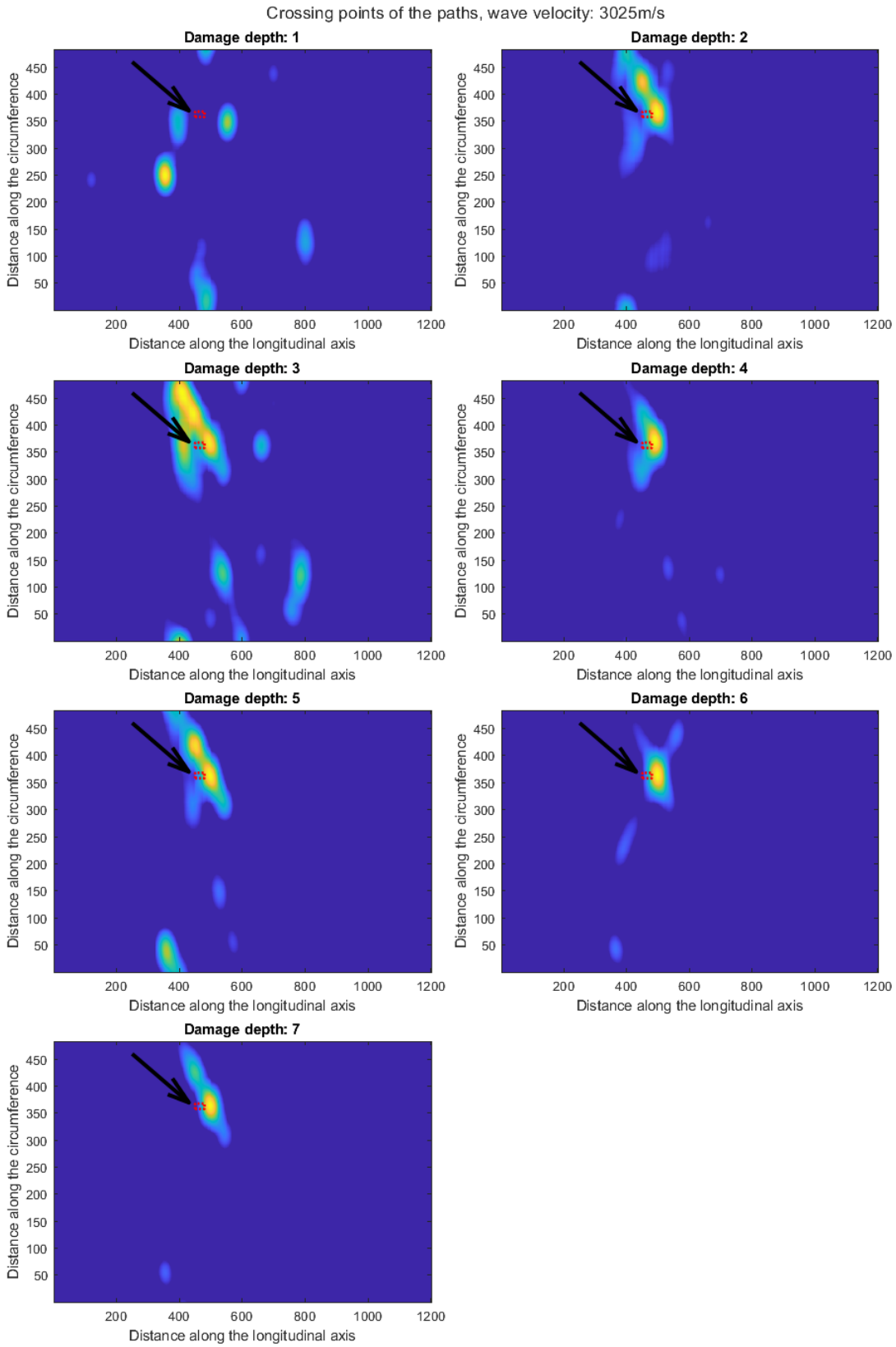


**Figure 4.11:** The crossing points of paths presented in figure 4.10 the frequency of the crossing areas is correlated with the damage location. The location of the defect is marked with red rectangle

## 4.3 Discussion

The lack of a training set ruled out the use of machine learning algorithms for this experiment, as the experiment was destructive in its nature. Despite of that, the system is capable of finding the defected location fairly well. The thresholds for peak detection were not adjusted based on the damage depth: this means that when the damage is more severe and there are more messy reflections, the simple model can not handle this and reports more false positives. The crossing point analysis still tends to find the approximate location of the defect, despite the amount of the possible paths being high.

When used in a case where the signals do not change so dramatically, from small 0.8 mm deep scratch to completely wide open hole, the thresholds can be adjusted so that the amount of false positives is smaller. In the end, this simple detection algorithm demonstrates the capabilities of the device network for defect localization. Even at its current state the highest probability for the defect to be situated according to the algorithm is pretty close to the actual location of the damage.

The results show a good longitudinal estimation of the defect location but a worse performance on the circumferential axis. This can be understood by the crossing point method, as it is more likely to find points crossing in the right approximate location along the longer axis; the changes are located between certain points and the biggest changes are prone to take place repeatably between the same transmitter and receiver. The worse resolution on circumferential axis can be explained by a larger amount of false positives caused by the non-refined algorithm detecting differences where there actually were no changes caused by the defect.

One possibility for the uncertainty is the effects taking place on the edge of the defect, as the interactions are simplified by using constant speed rays to represent the wave propagation. One possibility for inaccuracy is the possibility of interaction of already present defects or imperfections on the pipe that only appeared in the data during the damaging process when new reflected waves were interacting with them. Also it is possible that some of the odd results were caused by probe creep; that the signal was changing during the measurement series by change of adhesion between the probe and the pipe. As discussed in the theory section, more effort should be put in the mechanical coupling of the unit.

There is clearly room to improve the data analysis. The localization is not perfect but shows the possibilities of the developed system when paired with a machine learning algorithm. During the progress of this thesis the training was not possible due to lack of pipes to analyze and defect. It could have been interesting experiment to increase the amount of defects in the pipe to see if multiple damage locations can be distinguished

or would the system get confused and place its guess in completely wrong location.

When comparing the system and its results to the state of the art non destructive evaluation methods found in the literature and industry, the benefits are clear in terms of the system cost, it was surprising how small amount of physical materials, components and algorithm development was required to reach acceptable results. The system needs further development if it wants to compete against the ready products found in the industry and more research needs to be conducted with different pipe materials, fluids in the pipe, noisy environments and different geometries e.g. bends, t-junctions etc.

Even though the algorithm might never reach perfect localization, the system will be able to tell where the defect is located axially i.e. where it is in relation to the probes placed along the pipe. In real world applications the continuous monitoring will allow the detection of forming cracks in their early stages. In real world application just seeing a feature starting to form when compared to the base line, just in time domain like in figure 4.7, would be a reason enough to investigate the pipe section more carefully. The more careful investigation can then be done with more precise instruments, and the RAUS network would act as a early alarm system with its continuous monitoring and large spatial coverage.

# 5. Conclusions

Industries are interested in streamlining the processes, increasing throughput and avoiding the process down-time, one major cause of plant down-time is caused by unwanted leaks or clogging. So reliable and easy to implement systems to monitor pipelines are interesting topic in the industry. If the measurements can be performed completely externally without a need to stop the process and empty the pipeline, they can bring notable savings for the user. Use of inexpensive probes is interesting because they lower the threshold to apply for automated system diagnostic that requires no system down-time.

The affordability of the sensors allow for permanent installation, this allows continuous monitoring of the system. Continuous monitoring makes it easy to see any changes in the propagated sonic wave. More expensive systems are usually used by trained professionals and with portable set-ups. It is also very slow compared to a system that is monitoring the system in a permanent manner.

This thesis contained a proof-of-concept design of an inexpensive ultrasonic system for continuous pipeline monitoring, and a use case for damage localization with the developed system was successfully displayed. The use of this system has been proven for fouling localization in other publications. The possibility of combining system like one presented here with a system capable of cleaning pipelines from outside would be beneficial for many industries.

The key benefit of the system presented here is the permanent installation which reduces manual labor and makes repeated measurements over longer time periods possible.

The work taught the author electronic system design, considerations when doing measurements on a industry scale object, and data analysis when presenting the results. This system will be developed further to optimize the short comings presented in this work. These shortcomings include the transducer design, wireless triggering and training a machine learning algorithm to improve the damage localization.

The future holds various points to be refined and developed in the system, these include for example, the transducer design, the data transmission stream-lining, and training a machine learning algorithm to allow more versatile data analysis under

versatile circumstances. The transducer design will be an interesting topic to continue the development; finding an optimal backing to reduce the ringing and widening the band of the transducer. The wireless triggering can be achieved by utilizing narrow band MHz radio-modules and has already been achieved in the development of the system in work carried out after the measurements presented in this thesis.

# Bibliography


[1] S. S. Quarini J, "A review of fluid-driven pipeline pigs and their applications.," *Proceedings of the Institution of Mechanical Engineers, Part E: Journal of Process Mechanical Engineering.*, 2007.

[2] H. A. Kishawy and H. A. Gabbar, "Review of pipeline integrity management practices," *International Journal of Pressure Vessels and Piping*, vol. 87, no. 7, pp. 373–380, 2010.

[3] S. Sampath, K. L. Chaurasiya, P. Aryan, and B. Bhattacharya, "An innovative approach towards defect detection and localization in gas pipelines using integrated in-line inspection methods," *Journal of Natural Gas Science and Engineering*, vol. 90, p. 103933, 2021.

[4] M. E. Mountassir, G. Mourot, S. Yaacoubi, and D. Maquin, "Damage detection and localization in pipeline using sparse estimation of ultrasonic guided waves signals," *IFAC-PapersOnLine*, vol. 51, no. 24, pp. 941–948, 2018. 10th IFAC Symposium on Fault Detection, Supervision and Safety for Technical Processes SAFEPROCESS 2018.

[5] Z. Zhang, L. Zhang, M. Fu, D. Ozevin, and H. Yuan, "Study on leak localization for buried gas pipelines based on an acoustic method," *Tunnelling and Underground Space Technology*, vol. 120, p. 104247, 2022.

[6] S. C. Olisa, M. A. Khan, and A. Starr, "Review of current guided wave ultrasonic testing (gwut) limitations and future directions," *Sensors*, vol. 21, no. 3, 2021.

[7] H. Lais, P. S. Lowe, T.-H. Gan, L. C. Wrobel, and J. Kanfoud, "Characterization of the use of low frequency ultrasonic guided waves to detect fouling deposition in pipelines," *Sensors*, vol. 18, no. 7, 2018.

[8] R. Raisutis, O. Tumsys, E. Zukauskas, V. Samaitis, L. Draudviliene, and A. Jankauskas, "An inspection technique for steel pipes wall condition using ultrasonic guided helical waves and a limited number of transducers," *Materials*, vol. 16, no. 15, 2023.

[9] M. H. Zarifi, S. Deif, and M. Daneshmand, "Wireless passive rfid sensor for pipeline integrity monitoring," *Sensors and Actuators A: Physical*, vol. 261, pp. 24–29, 2017.

[10] D. Santos, M. A. Machado, J. Monteiro, J. P. Sousa, C. S. Proenca, F. S. Crivellaro, L. S. Rosado, and T. G. Santos, "Non-destructive inspection of high temperature piping combining ultrasound and eddy current testing," *Sensors*, vol. 23, no. 6, 2023.

[11] M. S. Rohani, "The development of non-contact laser and emat ultrasound measurement systems for hot steel." Unpublished, November 1996.

[12] S. Z. et al., "A methodological review of piezoelectric based acoustic wave generation and detection techniques for structural health monitoring," *International Journal of Aerospace Engineering*, 2013.

[13] X. Diao, Z. Chi, J. Jiang, A. Mebarki, L. Ni, Z. Wang, and Y. Hao, "Leak detection and location of flanged pipes: An integrated approach of principle component analysis and guided wave mode," *Safety Science*, vol. 129, p. 104809, 2020.

[14] S. Li, J. Zhang, D. Yan, P. Wang, Q. Huang, X. Zhao, Y. Cheng, Q. Zhou, N. Xiang, and T. Dong, "Leak detection and location in gas pipelines by extraction of cross spectrum of single non-dispersive guided wave modes," *Journal of Loss Prevention in the Process Industries*, vol. 44, pp. 255–262, 2016.

[15] M. D. Beard, *Guided Wave Inspection Of Embedded Cylindrical Structures*. PhD thesis, Imperial College of Science, Technology and Medicine, London, 2002.

[16] A. Spada, M. Capriotti, and F. Lanza di Scalea, "Global-local model for guided wave scattering problems with application to defect characterization in built-up composite structures," *International Journal of Solids and Structures*, vol. 182-183, pp. 267–280, 2020.

[17] J. D. Achenbach, *Wave Propagation in Elastic Solids*. Elsevier, 1975.

[18] S. Livadiotis, K. Sitaropoulos, A. Ebrahimkhanlou, and S. Salamone, "Acoustic emission monitoring of corrosion in steel pipes using lamb-type helical waves," *Structural Health Monitoring*, vol. 22, no. 2, pp. 1225–1236, 2023.

[19] E. Dale and L. Bond, *Ultrasonics: Fundamentals, Technologies and Applications 3rd Edition*. CRC Group, 2012.

[20] X. Liu, "Damage localization in plate-like structure using built-in pzt sensor network," *Smart structures and systems*, 2012.

[21] K. Ono, "Experimental determination of lamb-wave attenuation coefficients," *Applied Sciences*, vol. 12, no. 13, 2022.

[22] D. Alleyne and P. Cawley, "The interaction of lamb waves with defects," *IEEE Transactions on Ultrasonics, Ferroelectrics, and Frequency Control*, vol. 39, no. 3, pp. 381–397, 1992.

[23] S. H. . N. F. . D. G, "Emat pipe inspection with guided waves," *World of welding*, 2012.

[24] M. Harb and F.-G. Yuan, "Barely visible impact damage imaging using non-contact air-coupled transducer/laser doppler vibrometer system," *Structural Health Monitoring*, vol. 16, 11 2016.

[25] Scruby and Drain, *Laser Ultrasonics Techniques and Applications*. Routledge, 1990.

[26] J. Garcia-Martin, J. Gomez-Gil, and E. Vazquez-Sanchez, "Non-destructive techniques based on eddy current testing," *Sensors*, vol. 11, no. 3, pp. 2525–2565, 2011.

[27] Espressif, "ESP32 technical reference manual," 2018.

[28] Texas instruments SN54HC590A, *8-Bit binary counter*, 2003. Rev. F.

[29] G. Kossoff, "The effects of backing and matching on the performance of piezoelectric ceramic transducers," *IEEE Transactions on Sonics and Ultrasonics*, vol. 13, no. 1, pp. 20–30, 1966.

[30] A. V. Zinkevich, "Esp8266 microcontroller application in wireless synchronization tasks," in *2021 International Conference on Industrial Engineering, Applications and Manufacturing (ICIEAM)*, pp. 670–674, 2021.

[31] A. G. et al., "Multi-helical path exploitation in sparsity-based guided-wave imaging of defects in pipes," *Journal of Nondestructive Evaluation*, vol. 37, 3 2018.

[32] P. Salminen, J. Korsimaa, P. Ihalainen, D. Iablonskyi, A. Klami, A. Salmi, and E. Hæggström, "Affordable and wireless transducer network to detect fouling in pipes," in *2022 IEEE International Ultrasonics Symposium (IUS)*, pp. 1–4, 2022.

[33] NS (2023), Curve intersections (https://www.mathworks.com/matlabcentral/fileexchange/22441-curve-intersections).

# Appendix A. PCB layout

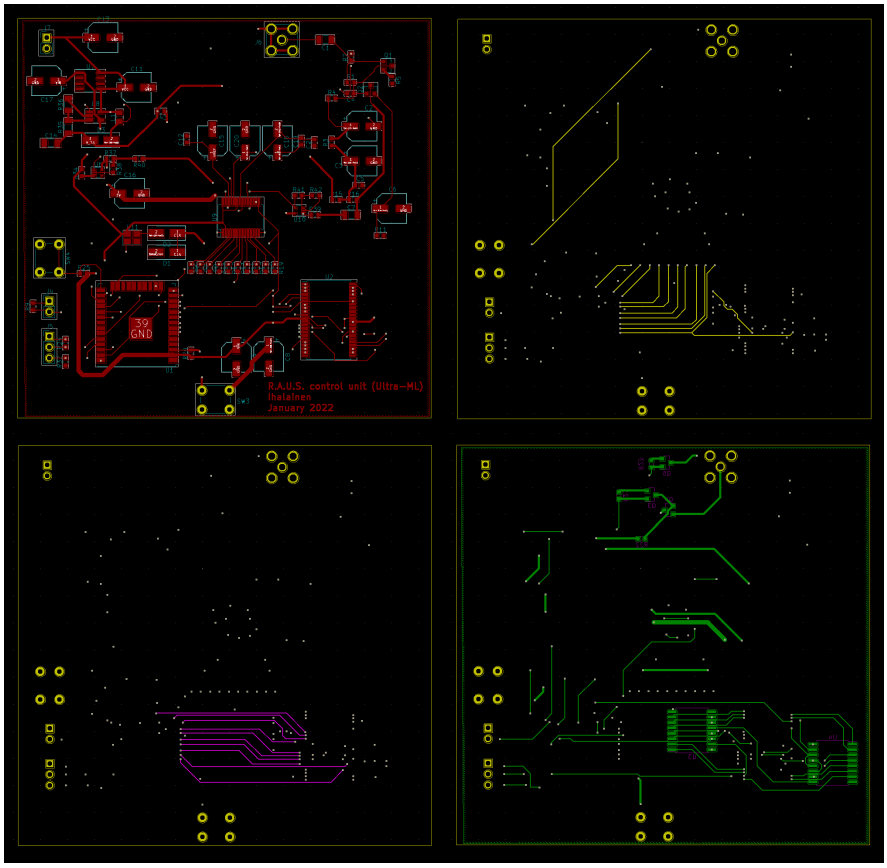


**Figure A.1:** The four layers of the device PCB